AIR FORCE INSTITUTE OF TECHNOLOGY

AIR UNIVERSITY
UNITED STATES AIR FORCE

A WIND-TUNNEL INVESTIGATION OF FORCES

ON CONES AT LOW MACH NUMBERS

THESIS

GAM 65B/AE/65-6 David Litwack
Capt USAF

SCHOOL OF ENGINEERING

WRIGHT-PATTERSON AIR FORCE BASE, OHIO

A WIND-TUNNEL INVESTIGATION OF FORCES ON CONES AT LOW MACH NUMBERS

THESIS

Presented to the Faculty of the School of Engineering of
the Air Force Institute of Technology
Air University
in Partial Fulfillment of the
Requirements for the Degree of
Master of Science

By

David Litwack, B.A.E.

Captain USAF

Graduate Aerospace-Mechanical Engineering

June 1965

Preface

The lack of subsonic aerodynamic force data on cones prompted the Aeronautical Engineering Department of the Air Force Institute of Technology to suggest that this investigation should be made. The purpose of this investigation was to obtain as much data as possible in the short time available and determine the areas in which a detailed analysis would be required.

The AFIT fourteen-inch wind tunnel with the three component wind tunnel balance system was used for this investigation. The nine aluminum cones were made by Mr. Hamilton of the AFIT shop. I wish to acknowledge the assistance of Mr. Barringer of the Aeronautical Engineering Laboratory in the operation and calibration of the equipment. I also, wish to express my appreciation to Professor H. C. Larsen and the Department of Aeronautical Engineering Staff for their suggestions and guidance during this investigation.

David Litwack

Contents

List of Figures

List of Tables

List of Symbols

Symbols	Meaning
C	..... Tunnel test section cross sectional area ($in.^2$)
C_D	..... Corrected drag coefficient
C_L	..... Corrected lift coefficient
$C_{M_{c.g.}}$	..... Corrected pitching moment coefficient about center of gravity of cone
$C_{M_{tr}}$	..... Corrected pitching moment coefficient about trunion
D	..... Corrected drag (lb.)
ΔD_B	..... Drag correction due to blockage (lb.)
D_b	..... Drag correction due to buoyancy (lb.)
D_m	..... Drag due to model (lb.)
D_s	..... Drag due to model supports (lb.)
I_m	..... Interference of model on supports
K_3	..... Body shape factor
L	..... Corrected lift (lb.)
L_m	..... Lift due to model (lb.)
L_s	..... Lift due to model supports (lb.)
M_{tr}	..... Pitching Moment about trunion (in.-lb.)
MFA	..... Model frontal area ($in.^2$)
R_e	..... Reynolds Number
S	..... Base area of cone ($in.^2$)
SFA	..... Strut and model mount frontal area ($in.^2$)
V	..... Volume of cone ($in.^3$)
a	..... Slope of the lift curve

Symbols	Meaning
c.g.	Cone center of gravity
d	Base diameter of cone (in.)
dp/dx	Static pressure gradient of test section (lb./ft.^{2}) / ft.
e	Tunnel blockage factor
h	Distance from bend in bent sting to center of gravity of cone (in.)
l	Distance from trunion to center of gravity of cone (in.)
m	Model cones
q	Corrected tunnel dynamic pressure (lb./ft.^{2})
q_u	Tunnel dynamic pressure read on meter (lb./ft.^{2})
α	Corrected angle of attack (deg.)
α_u	Angle of attack read on meter (deg.)
β	Angle between tunnel center line and model support (deg.)
δ	Boundary correction factor
μ	Coefficient of absolute viscosity (lb.-sec./ft.^{2})
ρ	Density of air (slugs/ft.^{3})
τ_1	Tunnel test section shape factor
τ_2	Streamline curvature effect on angle

Abstract

This investigation was conducted to obtain subsonic aerodynamic forces on cones. Nine aluminum cones varying in apex angle from 10° to 90° were tested in the Air Force Institute of Technology's fourteen-inch wind tunnel. Lift, drag and pitching moment were measured at angles of attack varying from -5° to 180° in 10° increments and at a dynamic pressure of up to 200 lb./ft.^{2}

The measured data was first corrected for tare and interference effects; three-dimensional wind-tunnel-boundary-corrections were then applied to correct the data to free-air conditions. This data is presented in graphical form as lift, drag and pitching moment coefficient versus angle of attack for each cone.

Due to the interactions of lift and drag on the pitching moment, the pitching moment data was unreliable and was not discussed in this report. A plot of drag coefficient versus Reynolds Number at each angle of attack for the 30° cone and the 60° cone showed the drag almost constant for each angle of attack over the small range of Reynolds Numbers tested ($Re = 1.5 \times 10^4$ to $Re = 5.7 \times 10^4$). The maximum lift to drag ratio for the three smallest cones (10° to 30° cone apex angle) occurred at an angle of attack between 30° to 40°; for every other cone (40° to 90° cone apex angle) the maximum L/D was at an angle of attack between 120° and 130°.

BLANK PAGE

I. Introduction

With the advent of the Apollo Space Program, there has been an increasing demand for development of a pilot controlled recovery and landing system for earthbound space vehicles. To achieve this goal, the aerodynamic forces produced by the vehicle in subsonic flight must be known.

All manned space vehicles currently considered are cone shaped and a search of the available literature revealed very little subsonic aerodynamic data on cones available at the present time. This lack of available data created the need for a compilation of information on subsonic aerodynamic forces on cones. This information could best be made available by performing a comprehensive testing program in a wind tunnel.

The purpose of this investigation was to make a general study of forces on cones at subsonic speeds and to establish the areas in which detailed studies would be required. To achieve this goal, nine cones varying in apex angle from 10° to 90° were tested in the AFIT fourteen-inch wind tunnel.

Lift, drag and pitching moment were measured through an angle of attack range of -5° to 180° in 10° increments. Three-dimensional-boundary- corrections were made on the force data; this force data was plotted versus angle of attack. A plot of drag coefficient versus Reynolds Number was made for the 30° cone and the 60° cone at each angle of attack. However, due to the small size of the cones and the speed limitation imposed by the drag scale, the Reynolds Number was small and no significant deviations were noted. The graphical

representations were reduced to coefficient form by using the base diameter of the cone as the characteristic length and are shown in Appendix A.

II. Apparatus

The apparatus used in this investigation consisted of the Air Force Institute of Technology's fourteen inch wind tunnel, the pyramidal balance system, the model mount and the nine model cones.

Wind Tunnel

The fourteen inch AFIT wind tunnel is a 1:17.45 scale model of the Wright Air Development Center's 20-foot wind tunnel. This tunnel is a closed circuit, single-return tunnel as shown in Fig. 1 with the exception of a modified conical diffuser insert (Ref. 2).

The test section has a 14.0 inch diameter, circular cross-section and is 32.5 inches long. The top half of the test section is removable to provide easy access to the model and the support system. (See Fig. 2)

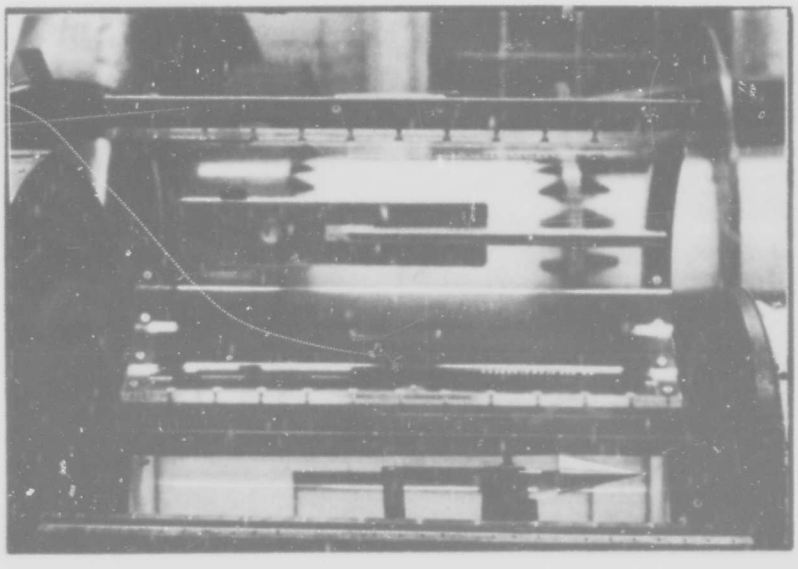

Fig. 2. Test section with top open.

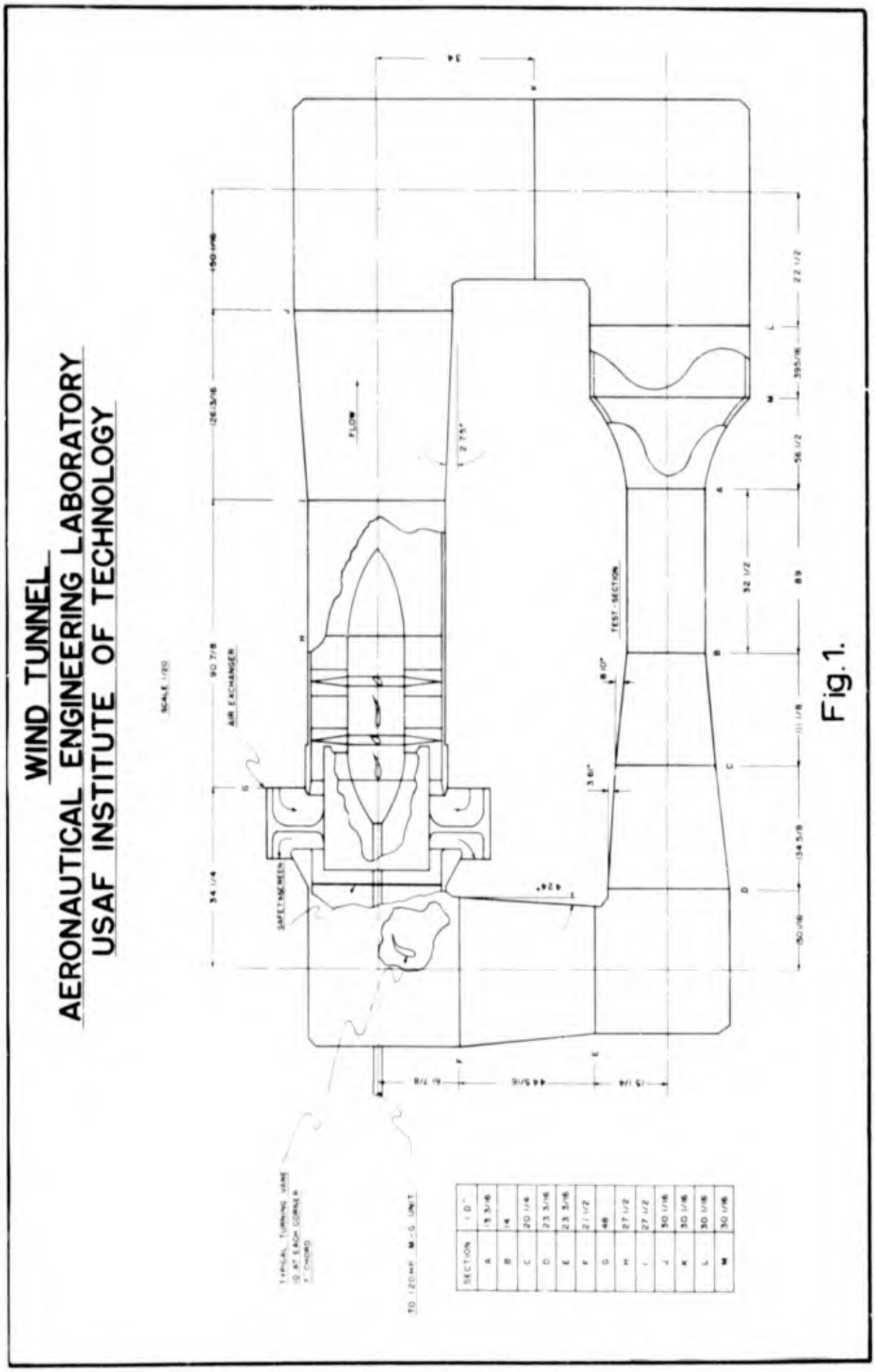
WIND TUNNEL
AERONAUTICAL ENGINEERING LABORATORY
USAF INSTITUTE OF TECHNOLOGY
SCALE 1/20
AIR EXCHANGER
SAFETY SCREEN
FLOW
TEST-SECTION
2.75°
8.10°
3.61°
4.24°
TYPICAL TURNING VANE
10 AT EACH CORNER
7" CHORD
TO 120 HP M-G UNIT
SECTION
A
B
C
D
E
F
G
H
I
J
K
L
M

Fig. 1.

Balance

The balance used for this investigation was the three degree of freedom pyramidal balance shown in Fig. 3. This balance is a null type balance with automatic scales and pitching mechanism; also, the balance system includes a remote indication and control panel. (See Fig. 4)

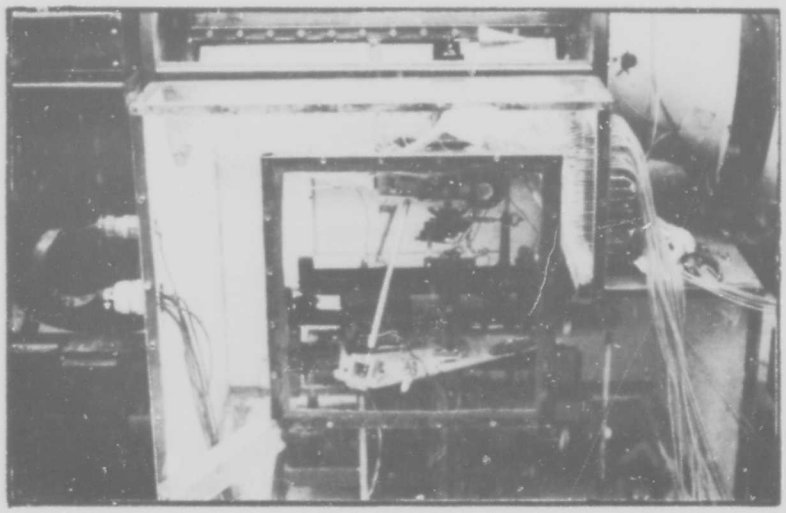

Fig. 3. Pyramidal balance.

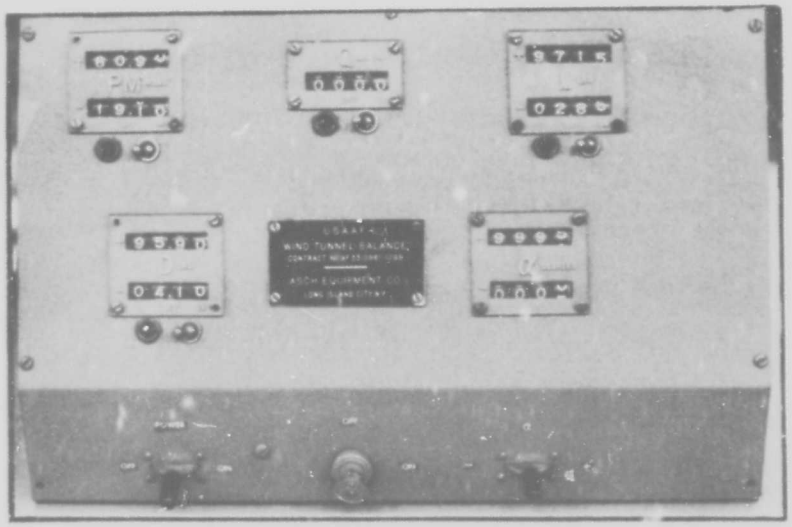

Fig. 4. Remote indication and control panel.

Lift, Drag and Pitching Moment are the three forces measured by the balance; in addition to these, the dynamic pressure is measured on a separate beam balance activated by a sylphon bellows. The load capacities and guaranteed accuracy of the balance are as follows;

Load	Capacity	Req'd Accuracy
Lift	+50/ -25 lbs.	$\pm$ 0.05 lbs.
Drag	$\pm$ 10 lbs.	$\pm$ 0.01 lbs.
Pitching Moment	$\pm$ 30 in.-lbs.	$\pm$ 0.05 in.lbs.
Dynamic Pressure	500 lbs./ ft.^{2}	$\pm$ 0.5 lbs./ ft.^{2}

Model Mount

The model mount system consisted of the three balance supports, the cross-member and the five model stings. (See Fig. 2)

The two front struts were rigidly mounted on the load table and enclosed by a fairing to eliminate wind forces from acting on the struts. The rear strut was connected to a motor activated pitching arm and was used to pitch the model through small angles.

The cross member was mounted on the three balance supports and served the two-fold purpose of holding the model stings and pitching the model by the action of the rear strut.

The five stings consisted of a straight sting and four stings bent at angles of 20°, 40°, 60° and 80° as shown in Fig. 5. To minimize the forces acting on the support system, the bent stings were used to pitch the model to large angles of attack.

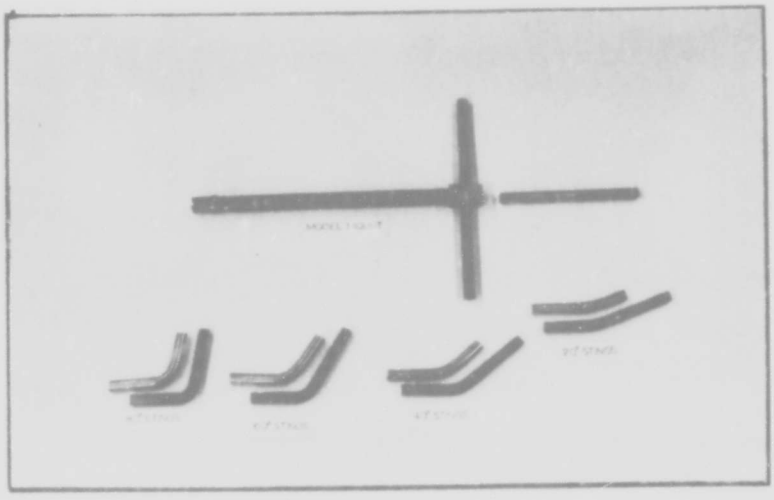

Fig. 5. Cross-Member and five stings.

Models

Nine cones varying in apex angle from 10^{o} to 90^{o} were used for this investigation and are shown in Fig. 6. The cones were constructed of aluminum for two reasons: first, to keep the models as light as possible; and second, to facilitate construction by the AFIT shop.

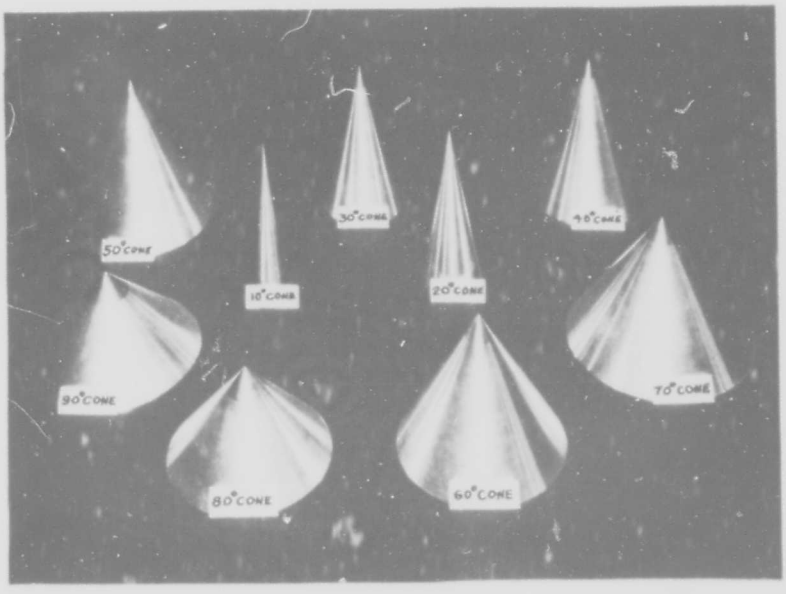

Fig. 6. Nine model cones.

Each cone had a threaded hole in the base for mounting on the stings to test between angles of attack of -5^{o} to 90^{o}. Each cone except the 10^{o} cone and the 20^{o} cone had a removable brass nosepiece which was removed for mounting the cone for tare runs and testing between angles of attack of 100^{o} to 180^{o}.

A maximum base diameter of approximately 4 inches and a maximum length of 4 inches were used to design the model cones. These limitations were imposed to confine the model to the test section area which had the least vertical variation of dynamic pressure (Ref. 2) and to minimize tunnel boundary corrections.

The specifications on each model cone tested were tabulated and are listed in appendix C.

III. Procedures

Calibration of Equipment

The tunnel speed was calibrated by comparing the electrical read-out to the measured pressure difference in the test section (manometer reading of total pressure minus static pressure) over the entire speed range in increments of q = 25 lb./ft.^{2} This data was plotted (Fig. 40) and the slope of the curve used to determine the accuracy of the system. The q scale was found to read 1.0% below the actual q; this deviation was corrected when the tunnel speed was set for each run throughout the test program.

The lift, drag and pitching moment scales were calibrated by loading the model mount with known weights and recording the balance read-outs. Calibration curves were drawn for each force component to determine the accuracy of the balance, as was done for the q scale. (See Fig. 37 - 39.)

The weights for the lift calibration were hung along the center-line of the model mount (Fig. 7.) to also measure any drag or pitching moment due to lift. No interaction of forces was noted and the lift

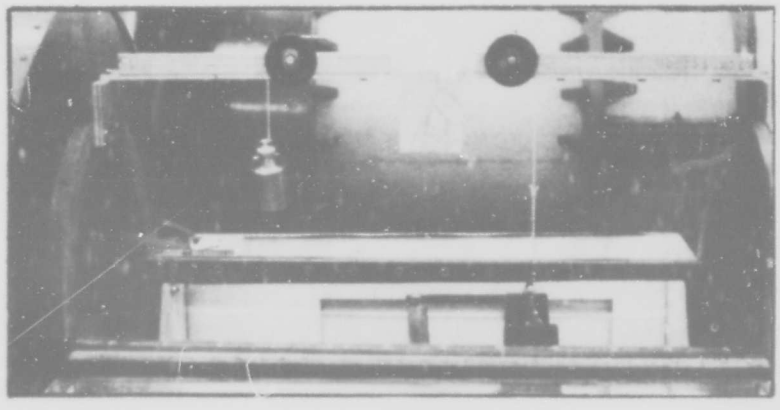

Fig. 7. Calibration of lift scale.

scale was found to record within the guaranteed accuracy of the balance system.

The drag scale was loaded as shown in Fig. 8 and although no interaction of forces was measured, the drag calibration curve showed that the actual drag was 1.0% higher than the recorded drag. This deviation was corrected in the data reduction.

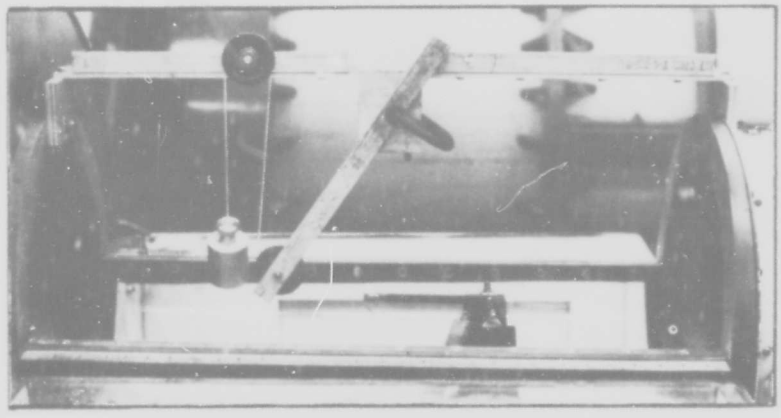

Fig. 8. Calibration of drag scale

Weights were hung an equal distance on either side of the model mount centerline and in opposite directions in order to load the balance in pure pitching moment. (See Fig. 9.) The pitching moment scale was within the guaranteed accuracy of the balance.

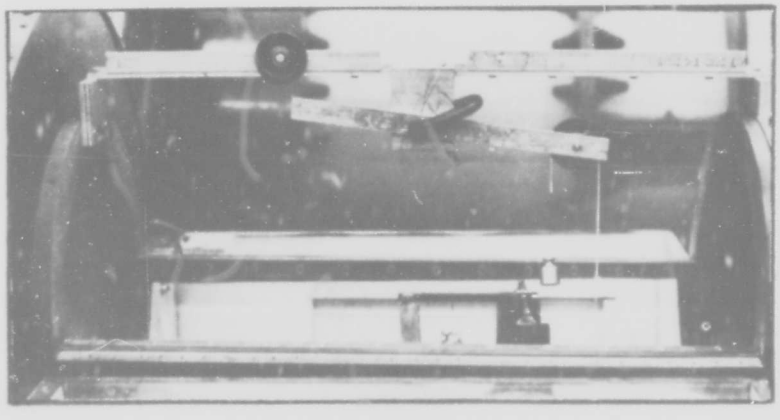

Fig. 9. Calibration of pitching moment scale

To calibrate the angle of attack indicator, an inclinometer was used to set the model at each desired angle of attack. The corresponding angle of attack indication was then recorded so that each angle could be repeated throughout the test program.

Model Test

For tests conducted in the angle of attack range from -5° to 90°, the stings were screwed into the base of the cone. The sting was then inserted into the front of the model mount and secured by tightening a set screw which fitted into a countersunk hole in the sting. (See Fig. 10) This method of attachment produced the same angle of attack each time the sting was used.

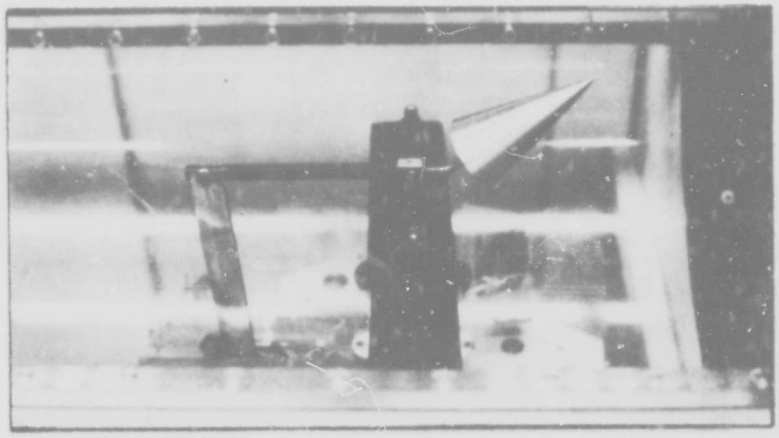

Fig. 10. Model installation ($\alpha = 40^{\circ}$)

Upon completion of the model installation, the upper half of the tunnel was secured in place. Zero readings of all scales were recorded and the tunnel was set at the test dynamic pressure and allowed to stabilize. Readings were then taken of lift, drag and pitching moment. Then, depending upon the particular test being run, one of the

following steps was performed; 1. Changing the tunnel speed. 2. Changing the angle of attack by the pitching arm. 3. Shutting down the tunnel. After tunnel shut down, another zero reading of each scale was taken for comparison with the readings taken prior to the run. The upper half of the tunnel test section was then removed and the angle of attack changed by installing the model with another sting.

In order to evaluate the tare forces and interference effects by the model on the support systems, the model had to be supported in its normal position but unattached to the balance. To accomplish this, a thin steel bar was suspended from the top of the tunnel test section to hold the cone in the proper position. The cone nose section was removed and the cone attached at the front end to the steel bar by an angle bracket as shown in Fig. 11. By supporting the model in this manner, the assumption was made that the steel bar did not influence the flow over the support system.

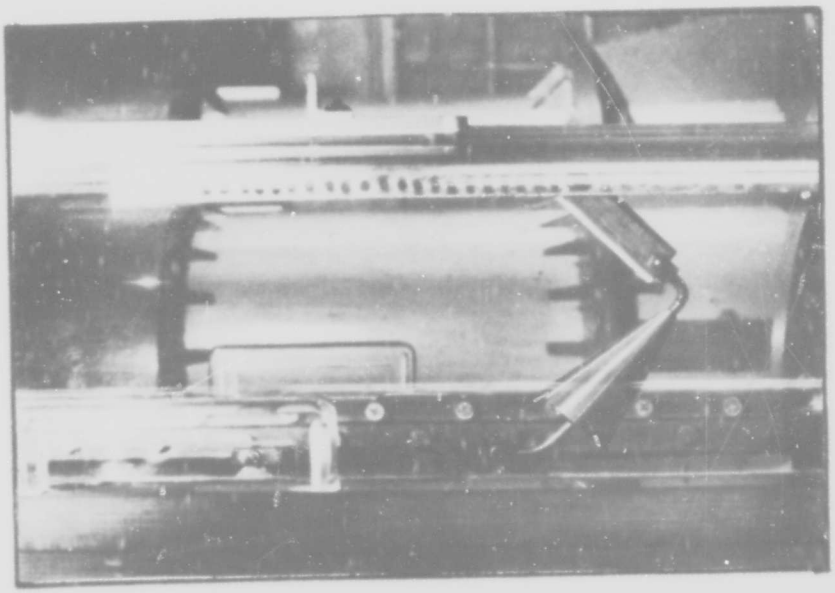

Fig. 11. Model installation for tare ($\alpha = 40^{\circ}$).

Although this method permitted the model to be held in the test section at any desired angle, exact positioning was difficult and time consuming.

Angles of attack between 100^{o} and 180^{o} were established by removing the tip of the cone and attaching the front end of the cone to the sting. (See Fig. 12.) The procedure for obtaining force data on the model was exactly the same as for the angle of attack range of -5^{o} to 90^{o}.

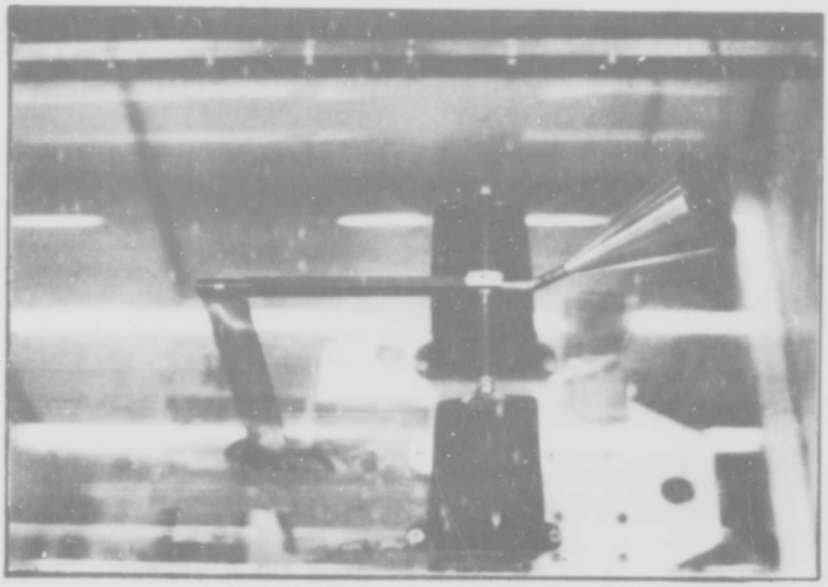

Fig. 12. Model installation ($\alpha = 140^{o}$)

The 10^{o} cone and 20^{o} cone did not have removable nose sections and a slightly different procedure was used to obtain the tare and interference forces. First, the tunnel was run with the model attached to the model mount and a steel rod supported from the upper half of the test section placed just behind the model as shown in Fig. 13. Then, the tunnel was run with the model attached to the steel rod as shown in Fig. 14 and the forces on the model obtained as previously

mentioned. Due to the small size of the 10° and 20° cones, it was assumed that the model had little effect on the support system. Above an angle of attack of 40° the steel rod was removed from the tunnel and the tare and interference forces were obtained with the model removed.

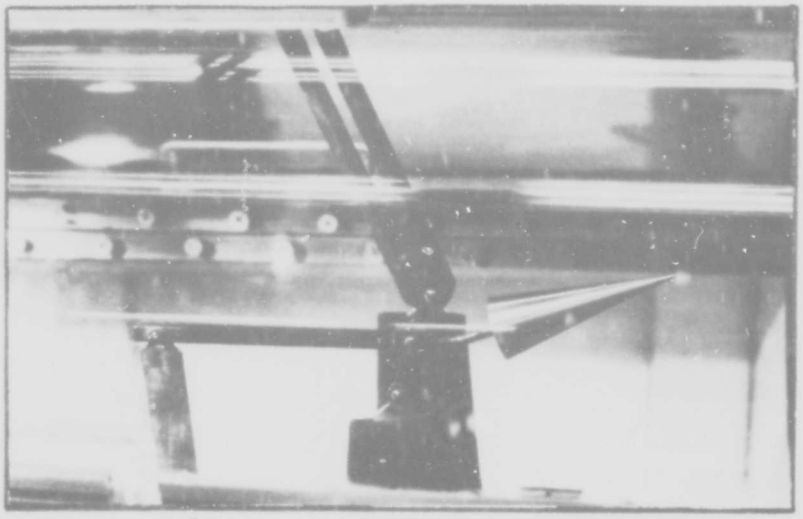

Fig. 13. 10° cone with upper support ($\alpha = 20^{\circ}$).

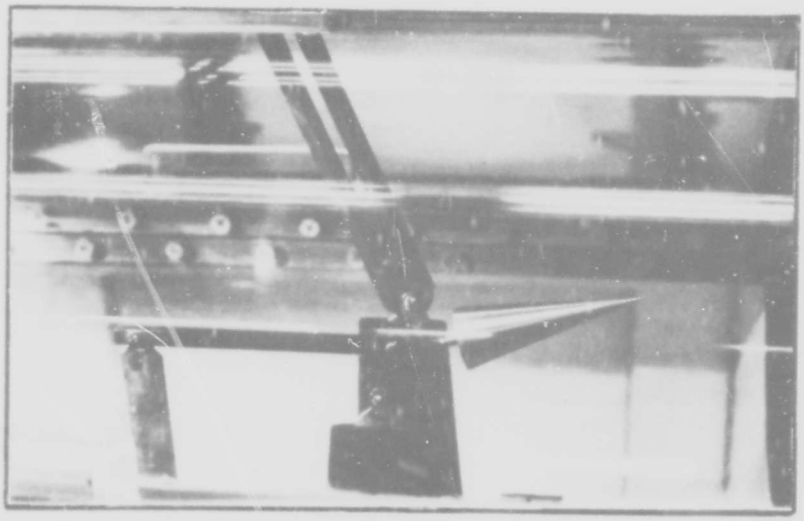

Fig. 14. 10° cone with upper support for tare ($\alpha = 20^{\circ}$).

The tunnel test speed was limited by the capacity of the drag scale for all except the two smallest cones. Table I gives a complete summary of the testing program utilized during this investigation

Table I. Test Program

cone	angle of attack range (deg.)	test speed lb./ft^2
10	-5 to 90	150
20	-5 to 90	150
30	-5 to 90	0 to 225
30	100 to 180	0 to 200
40	-5 to 90	150
40	100 to 180	100
50	-5 to 90	100
50	100 to 180	70
60	-5 to 90	0 to 150
60	100 to 180	75
70	-5 to 180	50
80	-5 to 180	75
90	-5 to 180	50

Data Reduction

The raw data was first corrected for tare forces and interference effects by subtracting the force data obtained with the model unattached to the balance from the force data obtained with the model attached to the balance. This operation yielded the uncorrected lift and drag acting on the cone and the uncorrected pitching moment

about the trunion. The data was then corrected for balance errors according to the calibration curves obtained from the calibration of the equipment. (See Fig. 37-39.) Three-dimensional wind-tunnel boundary corrections were then applied to correct the data to free-air conditions. The procedure used is summarized in Pope (Ref. 4:337) and is illustrated with a sample calculation in Appendix B.

The base diameter of each cone was used to express the forces in coefficient form and to compute the Reynolds Number for each speed.

IV. Accuracy of Measurements

The variables of this investigation were the tunnel speed, the balance system, the angle of attack, and the tare and interference effects. Each of these variables had to be examined for their accuracy and ability to repeat in order to determine the validity of the test results. The random errors induced by each component were estimated by statistical analysis and combined to obtain a standard deviation of the results.

Tunnel Speed

The tunnel speed was calibrated according to the procedure stated in section III. The guaranteed accuracy of the scale was 0.5 lb./ft.^{2} During the test program it was noted that a variation of q = 0.5 lb./ft.^{2} produced no significant change in lift or pitching moment and a change in drag of 0.1%. This is well within the accuracy of the drag scale; therefore, the tunnel speed could be set for each test with the required accuracy and reliability.

Balance System

The accuracy of the balance system under a static load was discussed in the Procedure section of this report. To determine the reliability of the system under aerodynamic loads, several runs were repeated on different days. The runs for each configuration were compared and the average deviations from the original runs were as follows: Lift 0.04 lb., drag .05 lb., and pitching moment 0.18 in.-lb. The air flow over the cone was probably slightly different each time a run was repeated; this produced the lift and drag deviations and

therefore, the balance system was considered to be repeatable within the accuracy of the experimental data for lift and drag.

The moment measured about the balance trunion consisted of the actual pitching moment, a moment due to lift and a moment due to drag. Repeated tests with the pitching moment proved unreliable; however, this was not due to the pitching moment scale but to changes in the measured pitching moment caused by the changes in the lift and drag.

Angle of Attack

The angle on each bent sting was determined by extending the straight portion and bent portion as shown in Fig. 15; measuring the length of the lines with a steel rule and then solving for the angle. This measurement was far more accurate than the readings from the angle of attack indicator which could be set only to within $\pm$ 0.1°.

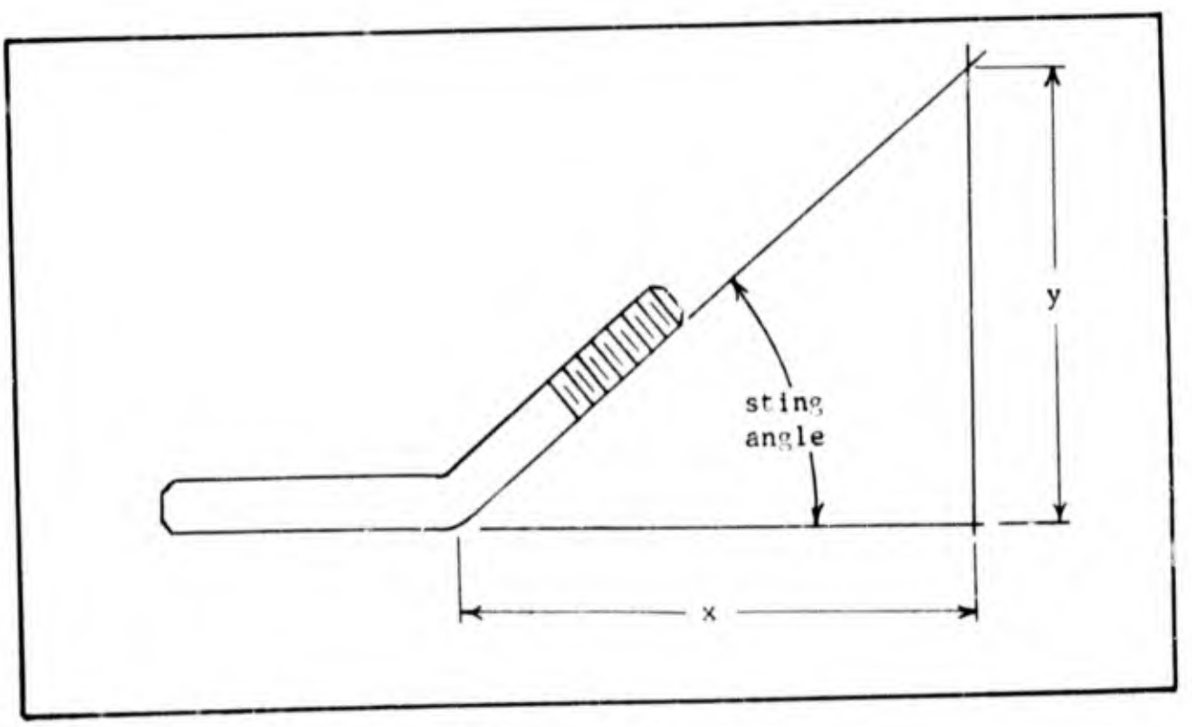

Fig. 15. Determination of sting angle.

It was observed visually that when the tunnel was set at the test speed, the angle of attack of the model had increased slightly. This increase was due to a small amount of "play" in the model mount and was measured with an inclinometer to be approximately 0.5^{o}.

For this investigation it was decided that an accuracy of $\pm 1^{o}$ would result in satisfactory results; therefore, the system was used without further refinement.

Tare and Interference

The measurement of tare forces and interference effects on the balance system was the most inaccurate of this investigation. This was almost entirely due to the method used to support the model in the tunnel for these measurements.

The model was supported from the upper half of the test section, as shown in Fig. 11; therefore, each angle of attack change required the removal of the upper half of the test section, the repositioning of the model and the replacement of the upper section. All settings were made visually with the aid of a tri-square; this procedure was very time consuming. Due to the limited time available, it was necessary to accept the position of the model whenever it was placed to within $\pm 3^{o}$ of the desired angle of attack.

Overall Accuracy

The variance used for the balance system was obtained from the static calibration data. For each of the other components, the variance was determined from the allowable accuracy stated in this section. Since the pitching moment could not be determined independently, no attempt was made to estimate the variance in the pitching

moment.

The results of this analysis are given in Table II below.

Table II. Variance of Results

Component	Variance C_L	Variance C_D
Tunnel Speed	0.000004	0.000005
Balance System	0.000142	0.000053
Angle of Attack	0.000098	0.000070
Tare and Interference	0.000114	0.000348
Total	0.000358	0.000476

The standard deviation for each component was found by taking the square root of the total variance. For the lift coefficient the standard deviation was 0.019 and for the drag coefficient the standard deviation was 0.022.

V. Discussion of Results

The results of this investigation are presented in graphical form in Appendix A. The base area of the cone was used to present the data in coefficient form. Coefficients determined from the frontal area would change the slopes of the curves but the general shapes would be the same. The discussion which follows would therefore, apply regardless of which method was used to represent the data.

Lift Coefficient Versus Angle of Attack

Examination of the curves for the various cones showed the lift coefficient curve slope to be almost linear in the angle of attack range of 0° to 50°. The slight curvature of the lift coefficient curves in this region is characteristic of bodies of revolution. Also, the lift coefficient curve slope in the range of $\alpha = 0^{\circ}$ to $\alpha = 60^{\circ}$ was noted to decrease as the cone angle increased as shown in Fig. 16a, 16b and 16c. It must be noted here that this is due mainly to the method of reducing the data to coefficient form.

A sharp break in the lift coefficient curves occurred at approximately $\alpha = 65^{\circ}$. This was probably due to flow attachment at the base and a "downward" flow around the cone. However, this could only be determined by flow visualization tests or a study of the pressure distribution on the cones; these tests were not made during this investigation.

All the cones exhibited a steep positive slope in the angle of attack range of 90° to approximately 120°. Also, at $\alpha = 120^{\circ}$ to 130°, the maximum lift coefficient occurred and increased in magnitude as the cone apex angle increased. It was in this range that the best

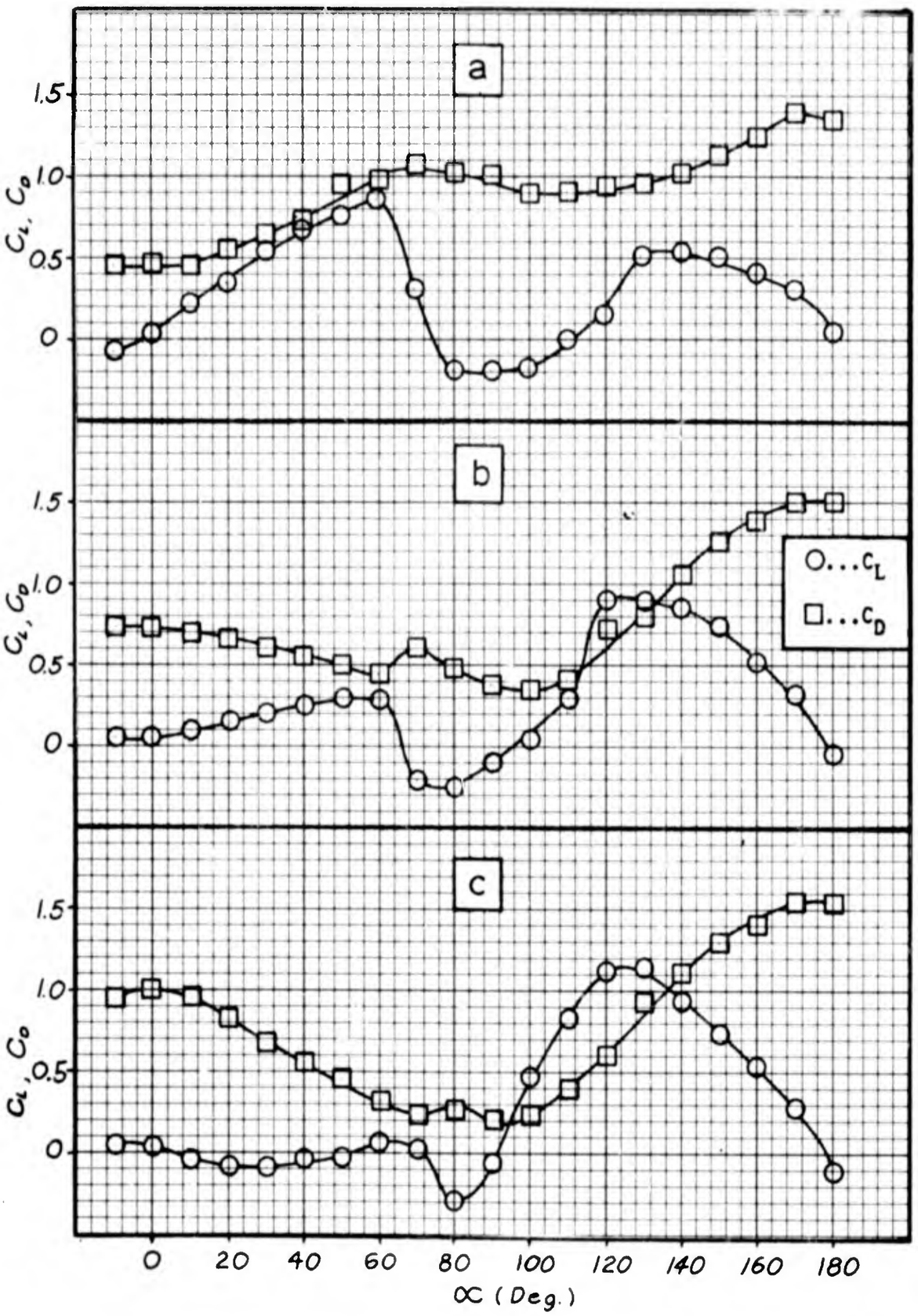

Fig. 16. Lift coefficient and drag coefficient plotted against angle of attack. a) For 30° cone, Re=36.8 x 10^4. b) For 60° cone, Re=41.2 x 10^4. c) For 90° cone, Re=40.1 x 10^4.

lift-to-drag ratios were obtained for all cones above an apex angle of 30°.

A small amount of lift was noted to exist for all cones at an angle of attack of 0°. This was probably due to the fact that an image system was not used, causing the flow to be nonaxi-symmetrical about the model and support system.

Drag Coefficient Versus Angle of Attack

The three smallest cones showed the similar characteristic of having an almost linear positive slope between an angle of attack of 10° to approximately 65°. The drag coefficient curves peaked at an angle of attack of about 70°; it was also at this point that the lift decreased rapidly. It is interesting to note that for the 30° cone at zero angle of attack, $C_D = 0.45$ compared to $C_D = 0.47$ for a sphere and at an angle of attack of 90°, $C_D = 1.0$ for the 30° cone compared to a $C_D = 1.2$ for a circular cylinder in two-dimensional cross-flow (Ref 4: 139).

The 40° cone had the characteristic peak at $\alpha = 70^{\circ}$; however, the slope of the drag coefficient curve between $\alpha = 0^{\circ}$ and $\alpha = 90^{\circ}$ was very shallow and resembled a transition to the characteristics of the larger cones. Between an angle of attack of 90° and 180°, the drag curve exhibited the same characteristics as those shown in Fig. 16.

The five largest cones (cone apex angles of 50° to 90°) had an almost linear, negative drag coefficient curve slope over an angle of attack range of 10° to 70°. This slope decreased with each increase in the cone angle. Another similarity in these drag coefficient curves was the characteristic "bump" which occurred at an angle of attack of

80^{o}, which in every case corresponded to the point of minimum lift.

An increase in the cone apex angle affected the flow separating from the base of the cone and caused the drag coefficient to increase as shown in Fig. 17 for $\alpha = 0^{o}$ (Ref 3: 3.17). At $\alpha = 180^{o}$, Fig. 17 shows the drag coefficient essentially constant at 1.58 and compares very well with a flat plate with a splitter device in the wake which has a $C_D = 1.6$ (Ref 3: 3.2).

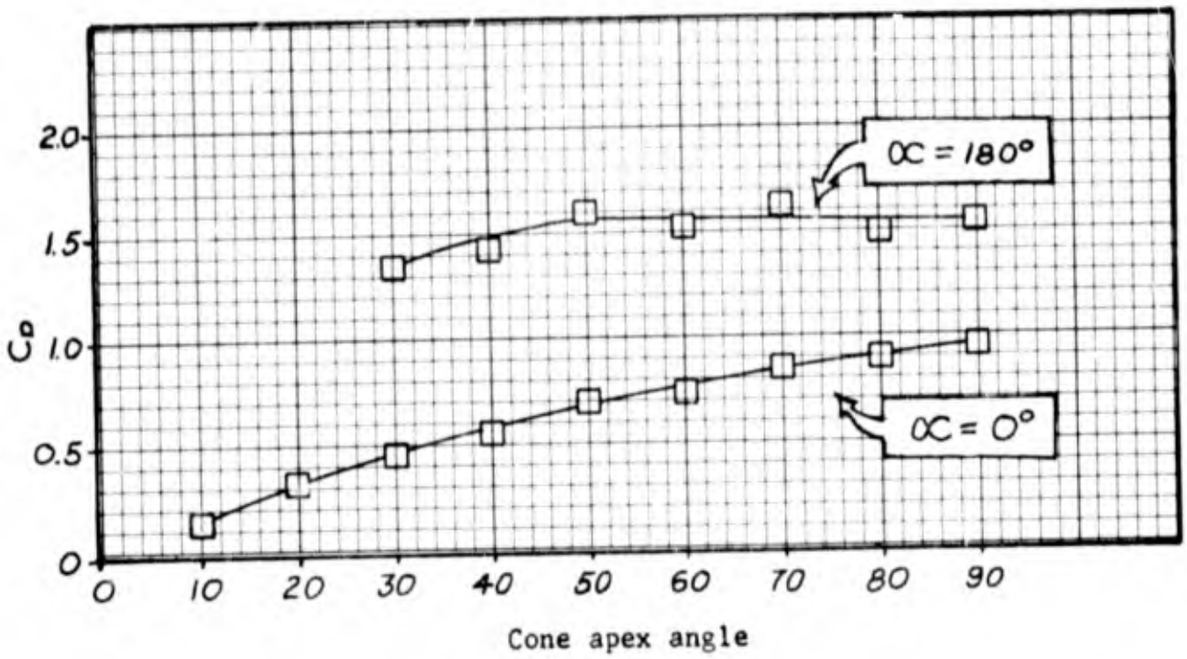

Fig. 17. Drag coefficients plotted against their cone apex angle at a constant angle of attack.

Drag Coefficient Versus Reynolds Number

Due to the limitations of the equipment, as discussed in the Procedure section of this report, the range of Reynolds Number was not as large as desired. The results for the 30^{o} cone shown in Fig. 20 and 21 show the drag coefficient to be essentially constant for each angle of attack over the range tested. The 60^{o} cone (Fig. 29) also exhibited a nearly constant drag coefficient with Reynolds Number for

each angle of attack.

A comparison was made between the results of this report and those of Eiffel for the 30° and 60° cones at a Reynolds Number of 2.3×10^{5} and a 0° angle of attack. This investigation produced a $C_D = 0.45$ for the 30° cone and a $C_D = 0.72$ for the 60° cone; Eiffel gave a $C_D = 0.37$ for the 30° cone and $C_D = 0.57$ for the 60° cone (Ref 1: 121). The drag coefficients in this study were higher than Eiffel's for the 30° and 60° cones by 18% and 26% respectively.

Hoerner noted that rounding sharp edges reduces the drag coefficient from between 50% to 90% depending on the shape of the afterbody (Ref 3: 313). The aluminum cones used in this investigation had an extremely sharp edge in comparison to the wooden cones used by Eiffel; this difference in construction was probably the major cause of the differences in the results.

Pitching Moment Coefficient Versus Angle of Attack

The inaccuracies involved in determining the pitching moment about the center-of-gravity of the cone, discussed in the Accuracy of Measurement section, caused a considerable spread in the points of $C_{M_{c.g.}}$ versus α. Due to this large spread, no attempt was made to draw any conclusions from this data or discuss these results in this report.

VI. Conclusions and Recommendations

The results of this investigation on forces on cones were considered satisfactory with the following exceptions: 1) The pitching moment coefficient measurements obtained were inaccurate. 2) The desired Reynolds Number range was not obtained. This general investigation pointed out several areas where a detailed investigation would be desired. One area was the angle of attack range between 40° and 70°. Another was the angle of attack range between 100° and 130°; this was the range in which the maximum lift to drag ratio occurred.

To obtain a more accurate measurement of the pitching moment, the cones will have to be mounted on the trunion center or on a sting balance capable of measuring forces to acceptable accuracy. The balance system should also allow the tunnel speed to be increased to obtain a Reynolds Number of at least 10^{6}.

The high drag obtained in this investigation could be reduced considerably by rounding the edge of the cone or adding a slightly curved afterbody.

As a result of this investigation the following recommendations for future tests are submitted.

1) Conduct a detailed investigation of the forces acting on cones between an angle of attack of 40° to 70° and between 100° and 130°.

2) Study the effects of tripping the boundary layer with a wire or a roughened surface.

3) Investigate the effects of adding a curved afterbody to the base of the cone.

4) Determine the effects of adding a blunt nose section to the cone.

5) Make a flow study about the cones with a hot-wire anemometer or a pressure rake survey to determine the area of separation or the flow detachment.

6) Conduct pressure distribution measurements on the side and base of the cone.

7) Measure the base pressure during force measurements.

8) Conduct a study of the flow in the wake.

Bibliography

1. Eiffel, G. Resistance of the Air and Aviation. Boston: Houghton, Mifflin and Co., 1913.

2. Gorman, Robert E. Diffuser Influence on Flow in the AFIT Wind Tunnel. Unpublished Thesis, Air Force Institute of Technology, 1958.

3. Hoerner, Sighard F. Fluid-Dynamic Drag. Published by Author, 1958.

4. Pope, Allen. Wind Tunnel Testing (Second Edition). New York: John Wiley and Sons, Inc., 1954.

5. Schlichting, Hermann. Boundary Layer Theory (Fourth Edition). New York: McGraw-Hill Book Co , Inc., 1960.

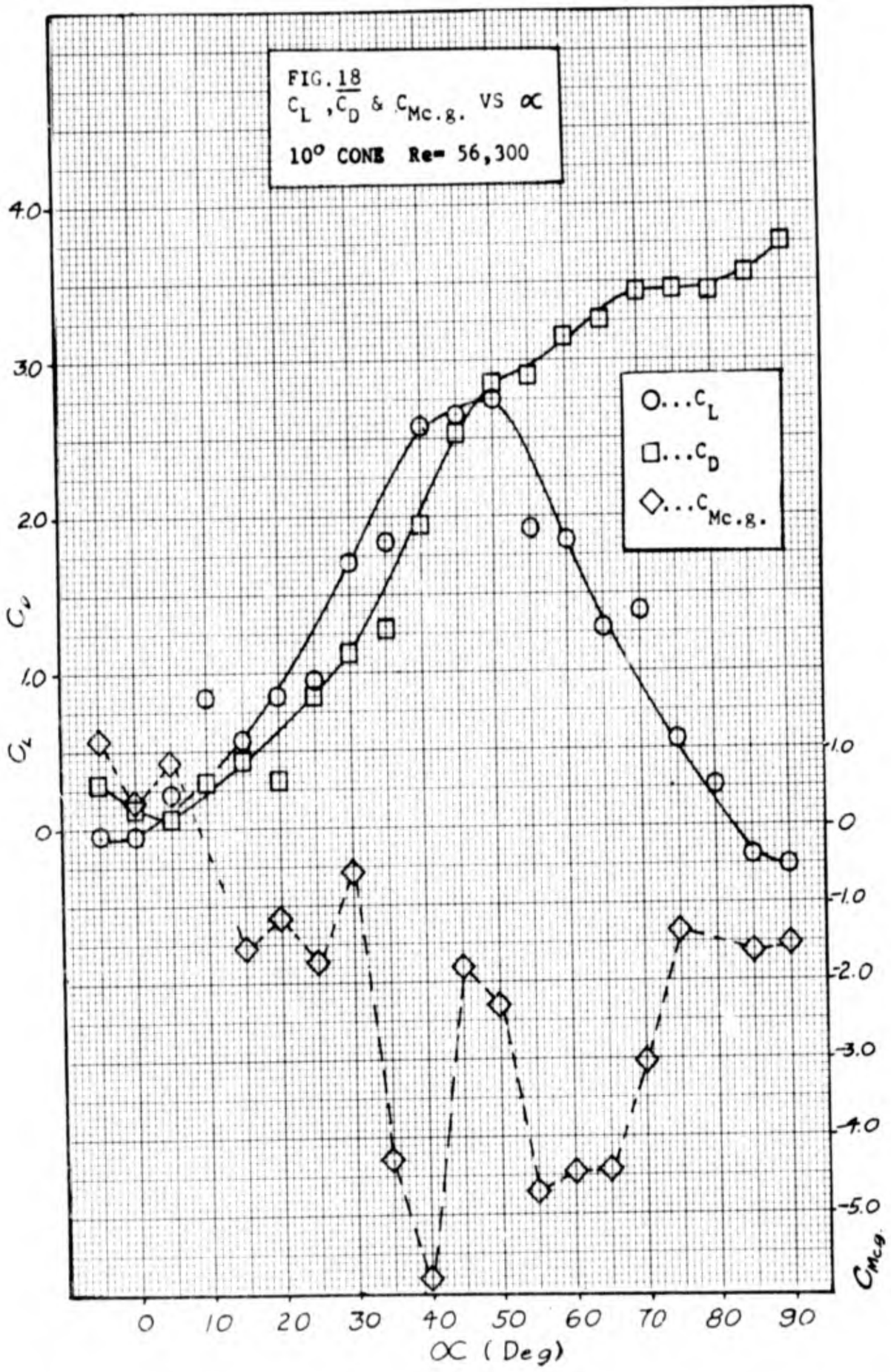
FIG. 18
C_L, C_D & $C_{Mc.g.}$ VS α
10° CONE Re= 56,300
O...C_L
□...C_D
◇...$C_{Mc.g.}$
4.0
3.0
2.0
1.0
0
C_L
C_D
1.0
0
-1.0
-2.0
-3.0
-4.0
-5.0
$C_{Mc.g.}$
0 10 20 30 40 50 60 70 80 90
α (Deg)

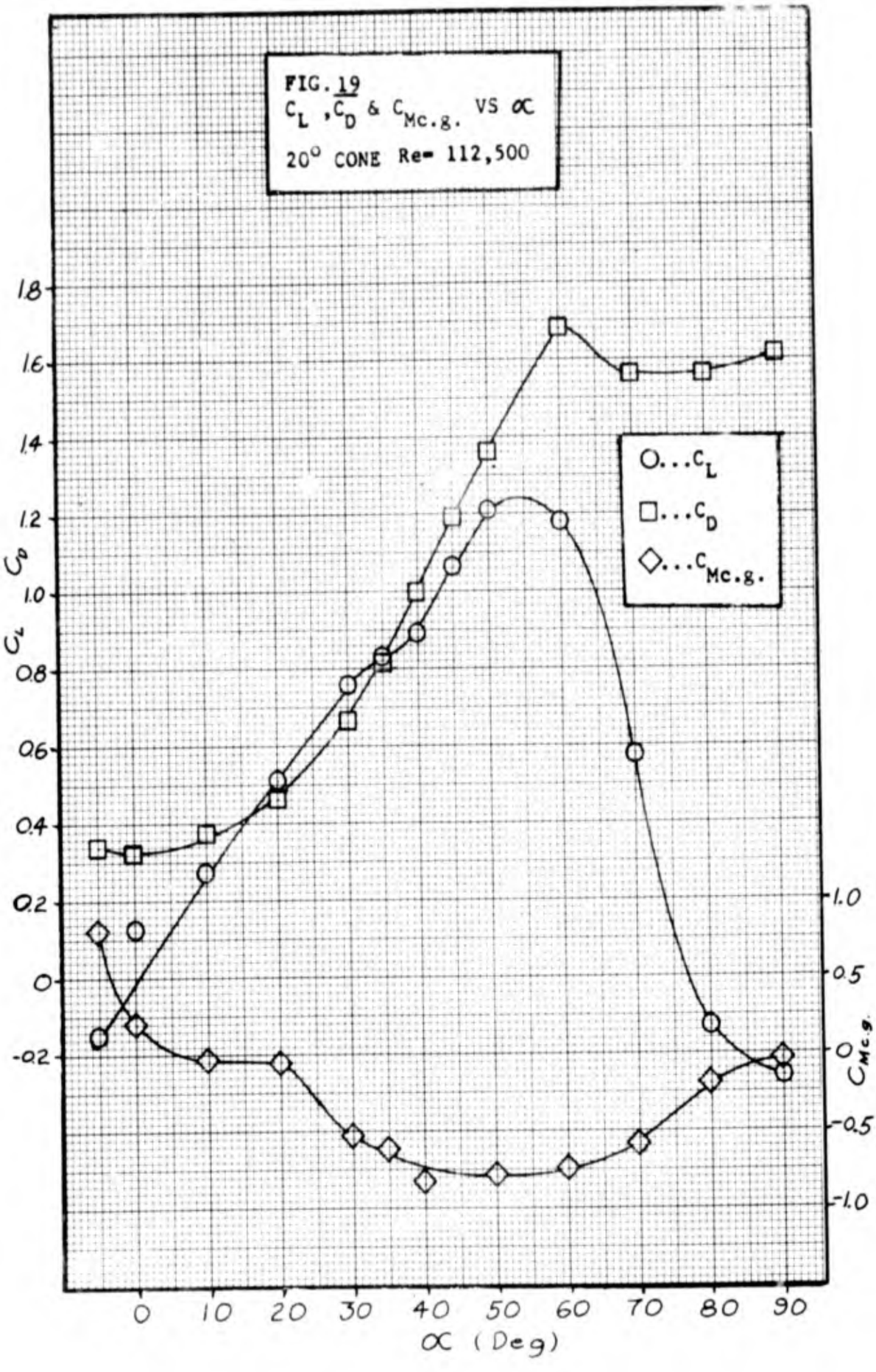
FIG. 19
C_L, C_D & $C_{Mc.g.}$ VS α
20° CONE Re= 112,500
O...C_L
□...C_D
◇...$C_{Mc.g.}$
C_D, C_L
1.8
1.6
1.4
1.2
1.0
0.8
0.6
0.4
0.2
0
-02
1.0
0.5
0
-0.5
-1.0
$C_{Mc.g.}$
0 10 20 30 40 50 60 70 80 90
α (Deg)

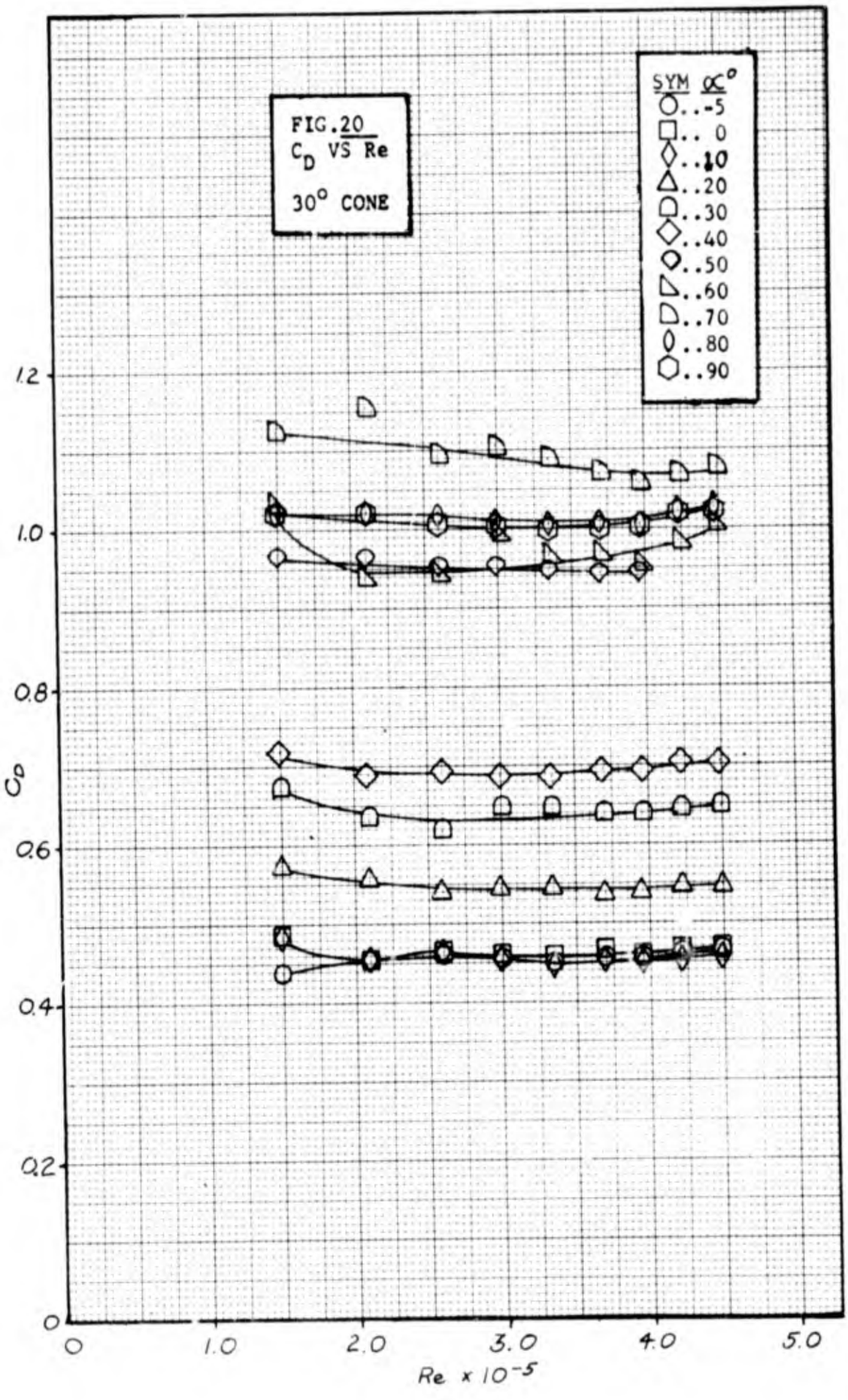
FIG. 20
C_D VS Re
30° CONE
SYM α°
-5
0
10
20
30
40
50
60
70
80
90
1.2
1.0
0.8
0.6
0.4
0.2
0
C_D
0
1.0
2.0
3.0
4.0
5.0
Re x 10^{-5}

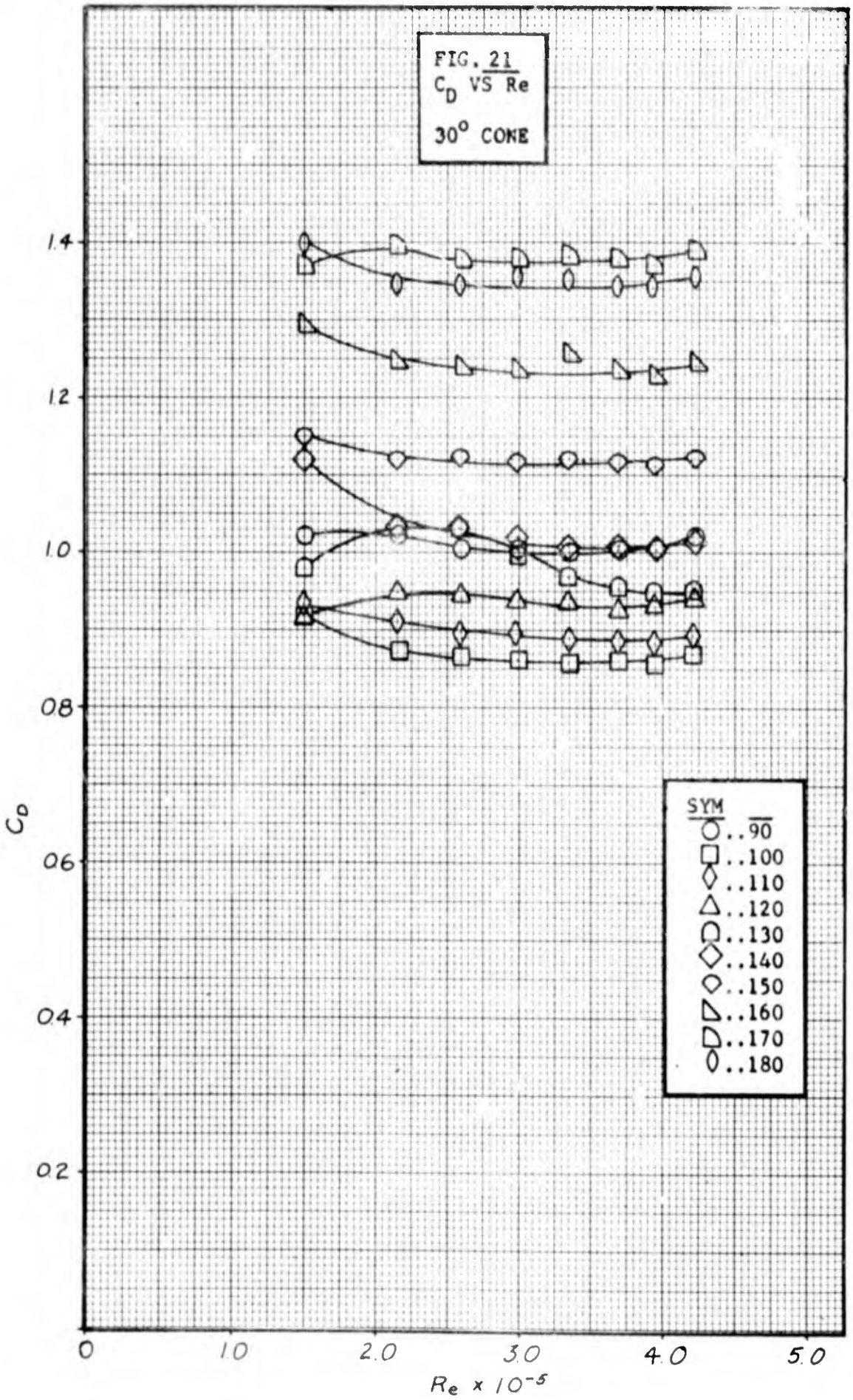
FIG. 21
C_D VS Re
30° CONE
1.4
1.2
1.0
08
06
04
02
C_D
0
1.0
2.0
3.0
4.0
5.0
Re x 10^{-5}
SYM
90
100
110
120
130
140
150
160
170
180

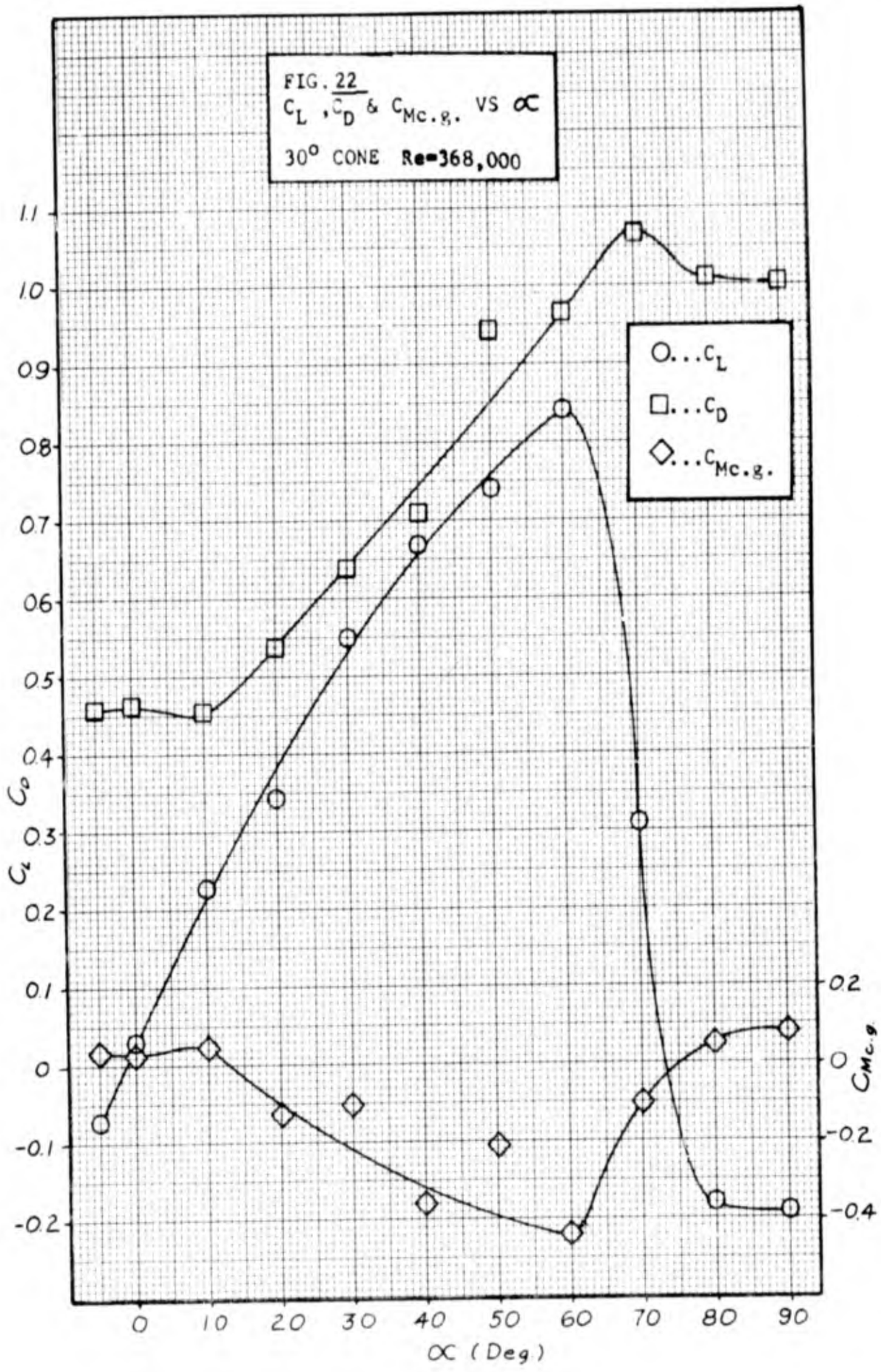
FIG. 22
C_L, C_D & $C_{Mc.g.}$ VS α
30° CONE Re=368,000
O...C_L
□...C_D
◇...$C_{Mc.g.}$
1.1
1.0
0.9
0.8
0.7
0.6
0.5
0.4
0.3
0.2
0.1
0
-0.1
-0.2
C_L C_D
0.2
0
-0.2
-0.4
$C_{Mc.g.}$
0 10 20 30 40 50 60 70 80 90
α (Deg)

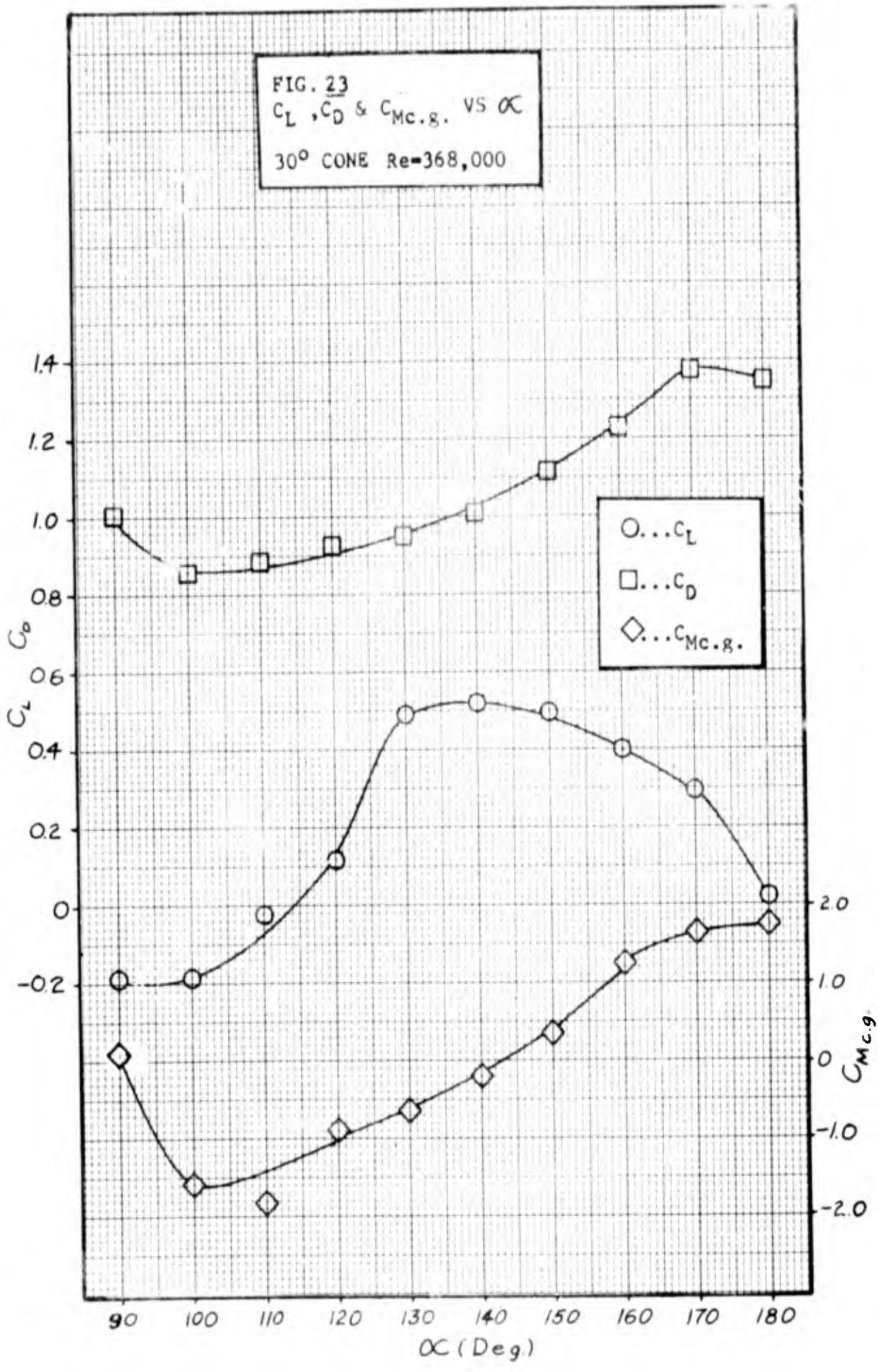
FIG. 23
C_L , C_D & $C_{Mc.g.}$ VS α
30° CONE Re=368,000
O...C_L
□...C_D
◇...$C_{Mc.g.}$
C_L C_D
$C_{Mc.g}$
1.4
1.2
1.0
0.8
0.6
0.4
0.2
0
-0.2
2.0
1.0
0
-1.0
-2.0
90
100
110
120
130
140
150
160
170
180
α (Deg.)

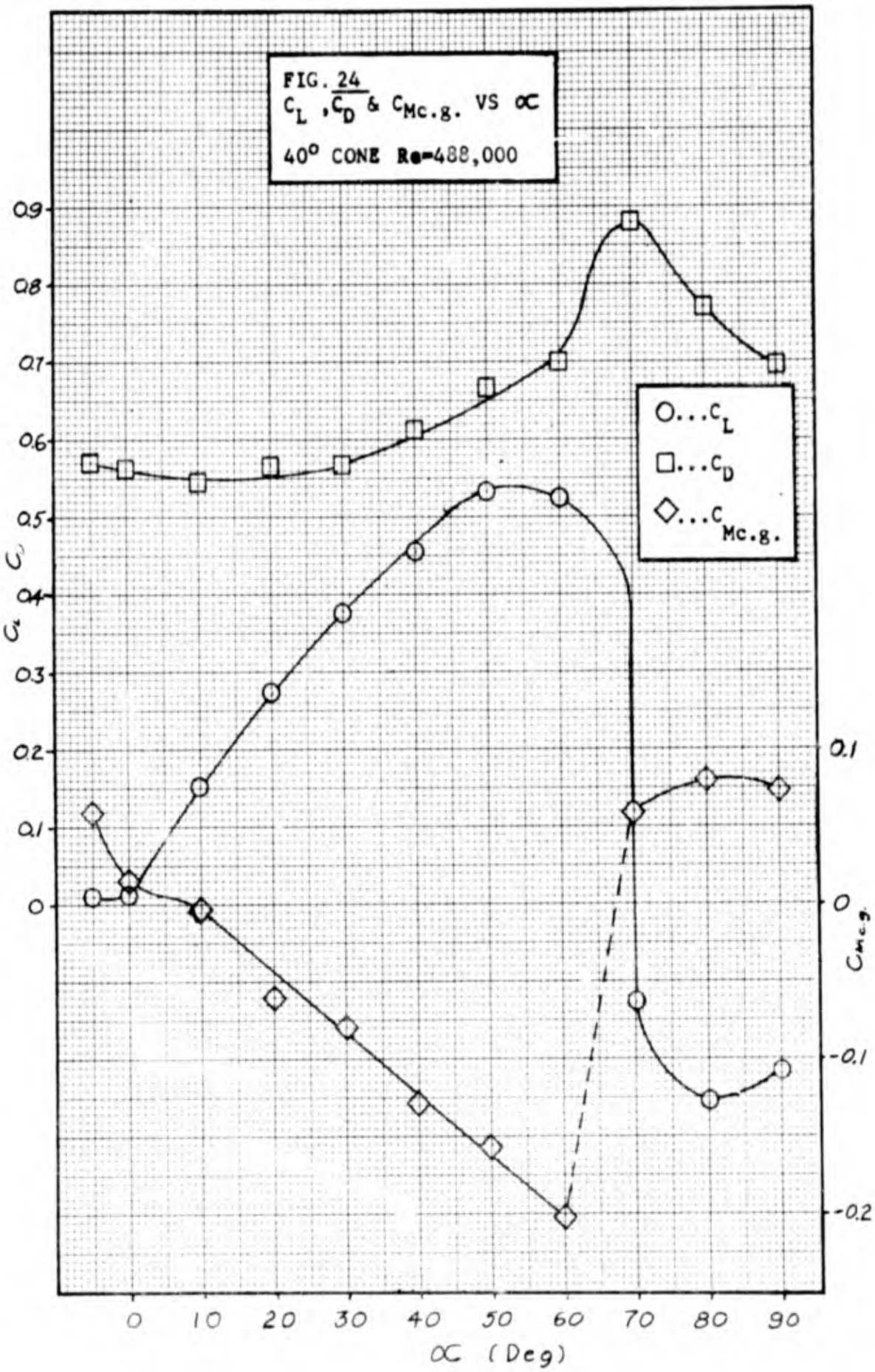
FIG. 24
C_L , C_D & $C_{Mc.g.}$ VS α
40° CONE Re=488,000
O...C_L
□...C_D
◇...$C_{Mc.g.}$
0.9
0.8
0.7
0.6
0.5
0.4
0.3
0.2
0.1
0
C_L , C_D
0.1
0
-0.1
-0.2
$C_{Mc.g.}$
0 10 20 30 40 50 60 70 80 90
α (Deg)

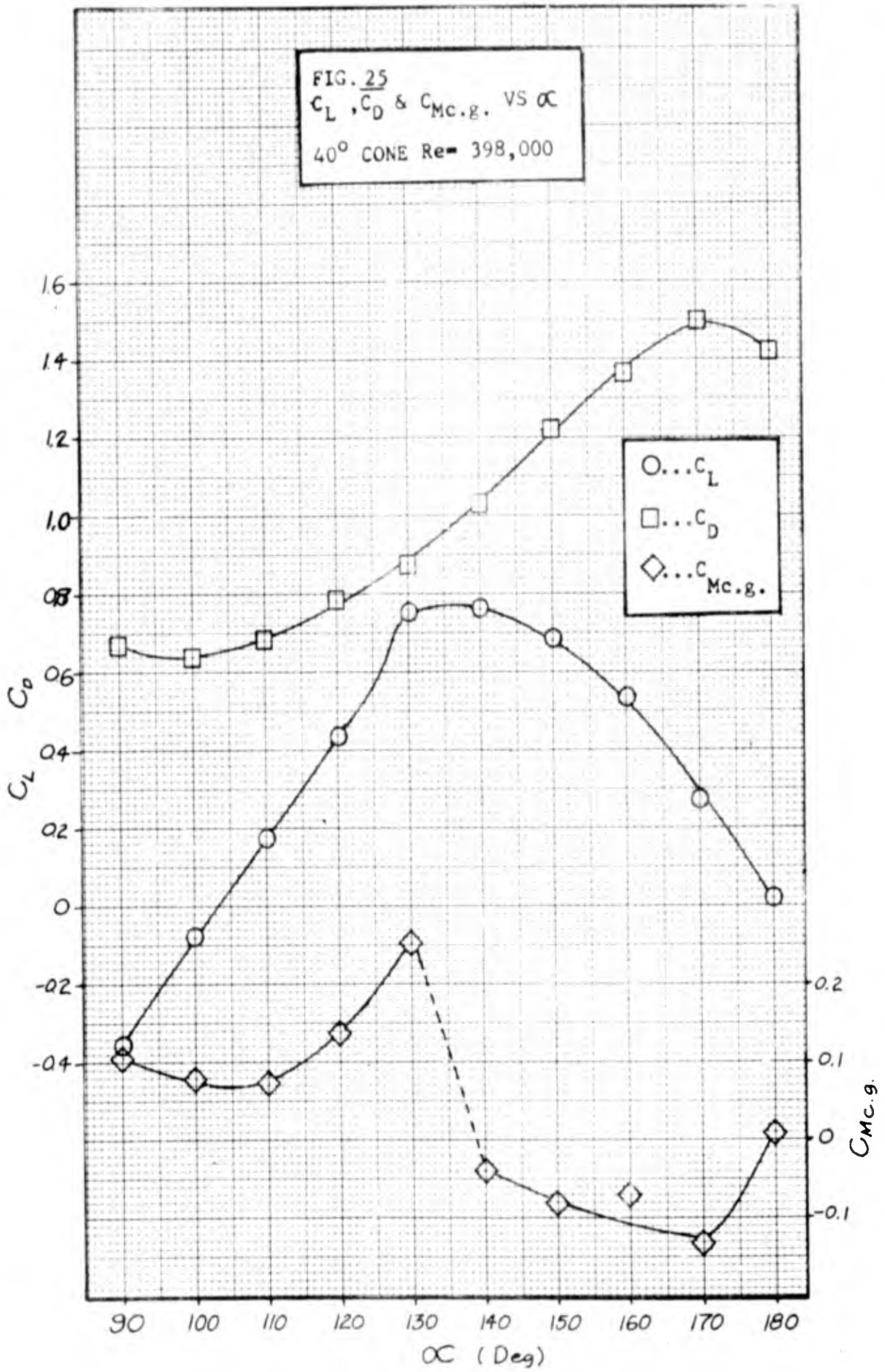
FIG. 25
C_L, C_D & $C_{Mc.g.}$ VS α
40° CONE Re= 398,000
O...C_L
□...C_D
◇...$C_{Mc.g.}$
C_D
C_L
$C_{Mc.g.}$
1.6
1.4
1.2
1.0
.8
.6
.4
.2
0
-.2
-.4
0.2
0.1
0
-0.1
90
100
110
120
130
140
150
160
170
180
α (Deg)

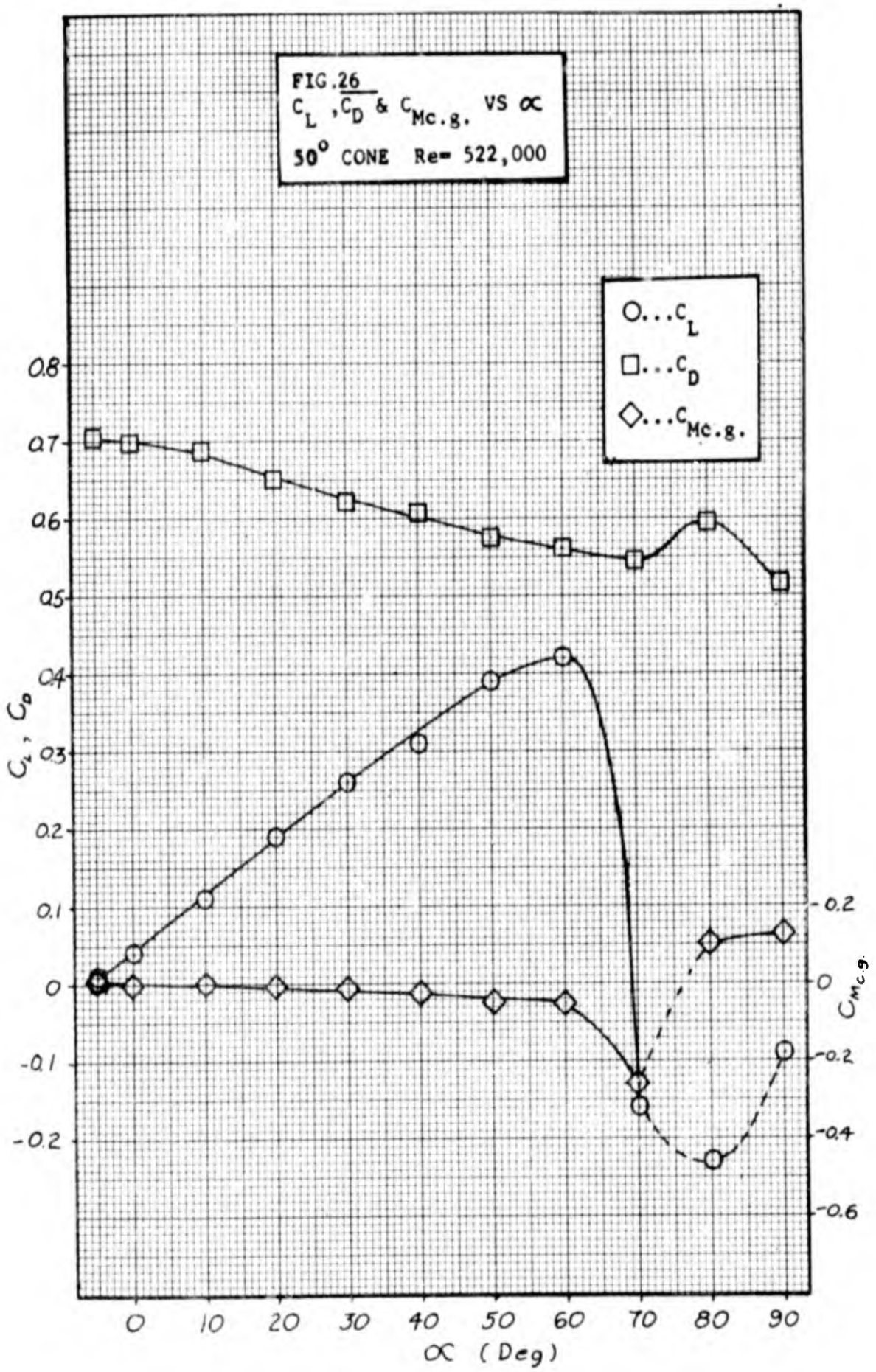
FIG.26
C_L, C_D & $C_{Mc.g.}$ VS α
50° CONE Re= 522,000
O...C_L
□...C_D
◇...$C_{Mc.g.}$
C_L, C_D
$C_{Mc.g.}$
α (Deg)
0.8
0.7
0.6
0.5
0.4
0.3
0.2
0.1
0
-0.1
-0.2
-0.2
0
-0.2
-0.4
-0.6
0
10
20
30
40
50
60
70
80
90

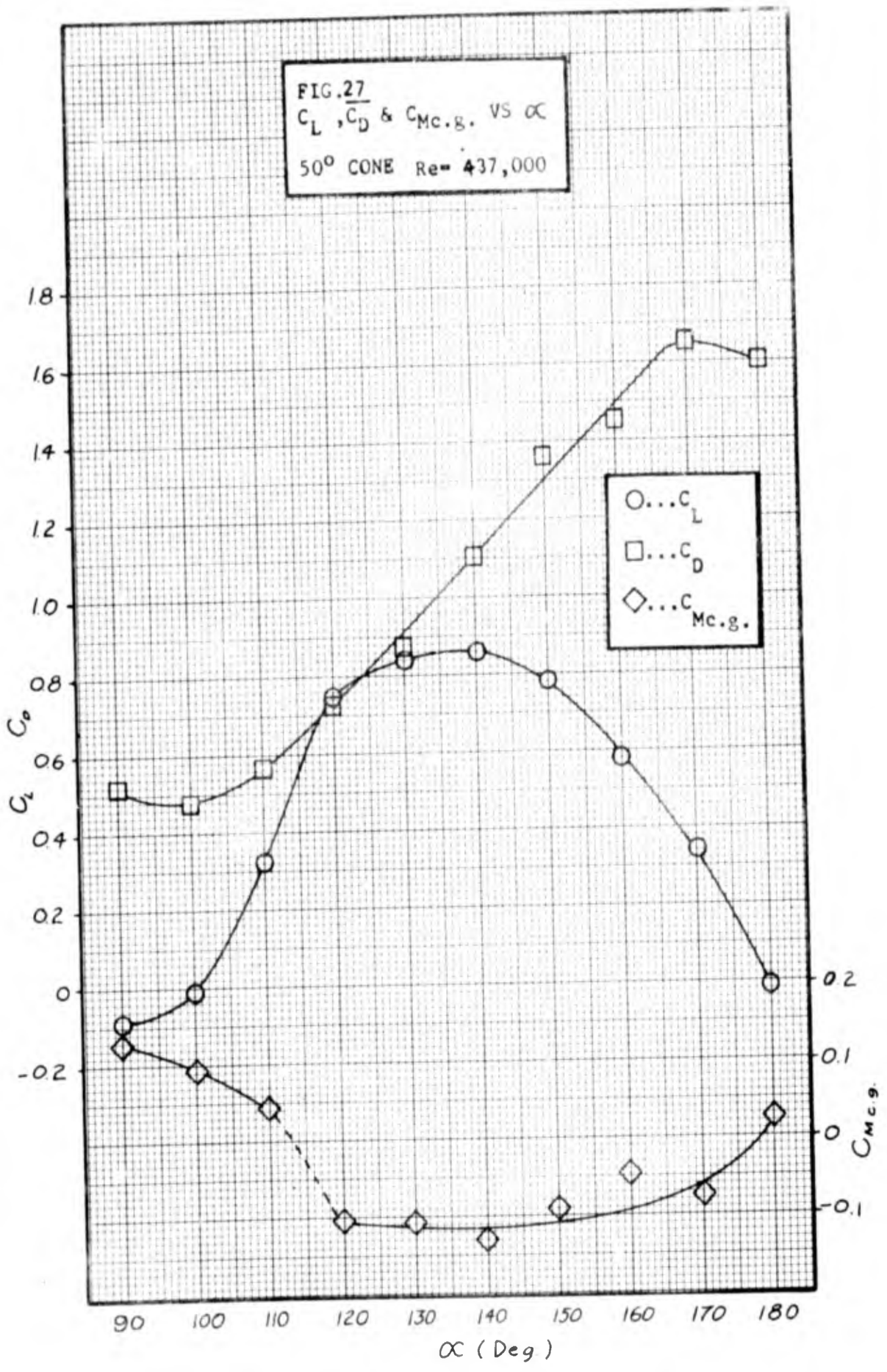
FIG.27
C_L , C_D & $C_{Mc.g.}$ VS α
50° CONE Re= 437,000
O...C_L
□...C_D
◇...$C_{Mc.g.}$
1.8
1.6
1.4
1.2
1.0
0.8
0.6
0.4
0.2
0
-0.2
C_o
C_L
0.2
0.1
0
-0.1
$C_{Mc.g.}$
90
100
110
120
130
140
150
160
170
180
α (Deg)

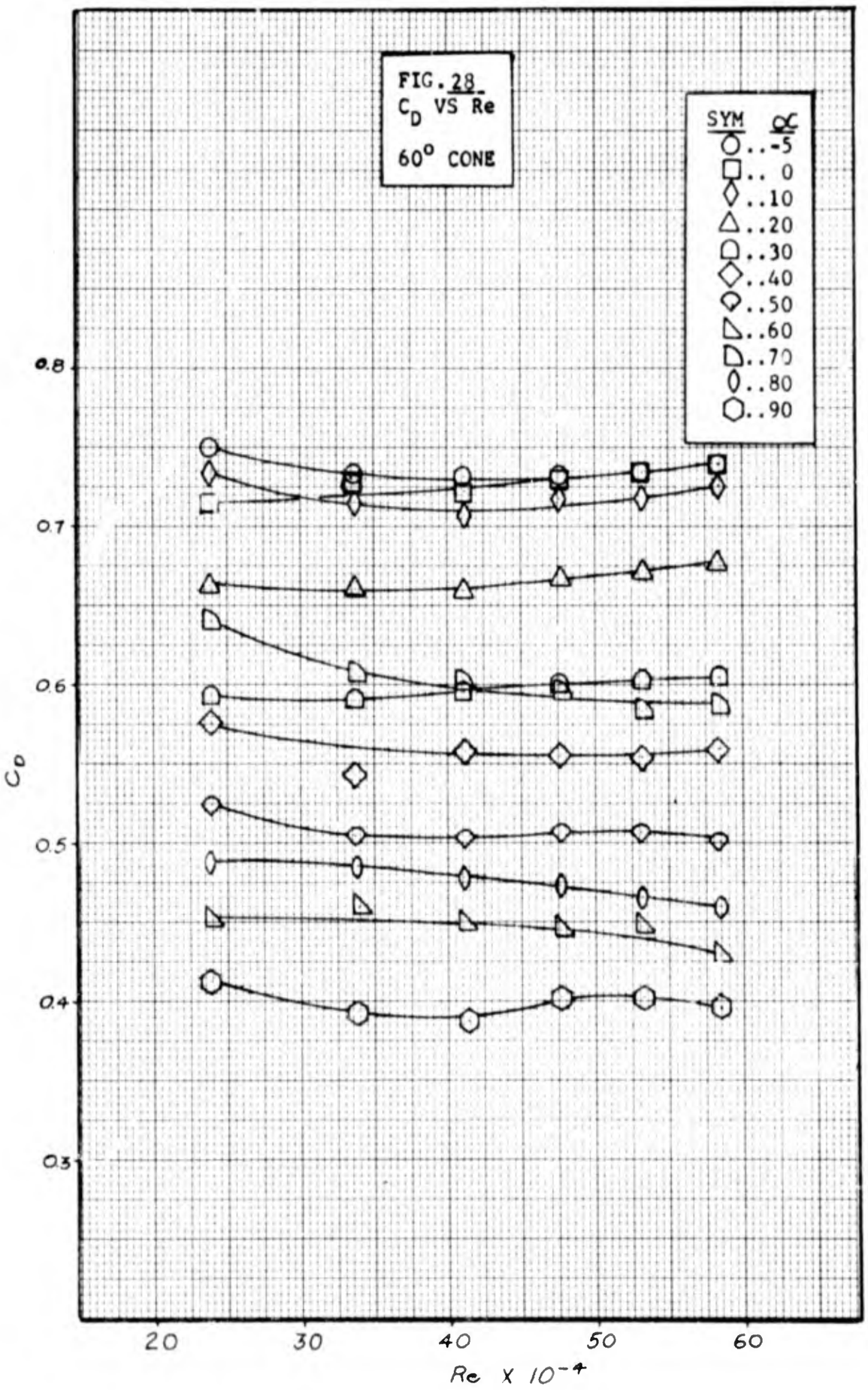
FIG. 28
C_D VS Re
60° CONE
SYM α
..-5
.. 0
..10
..20
..30
..40
..50
..60
..70
..80
..90
0.8
0.7
0.6
0.5
0.4
0.3
C_D
20
30
40
50
60
Re X 10^{-4}

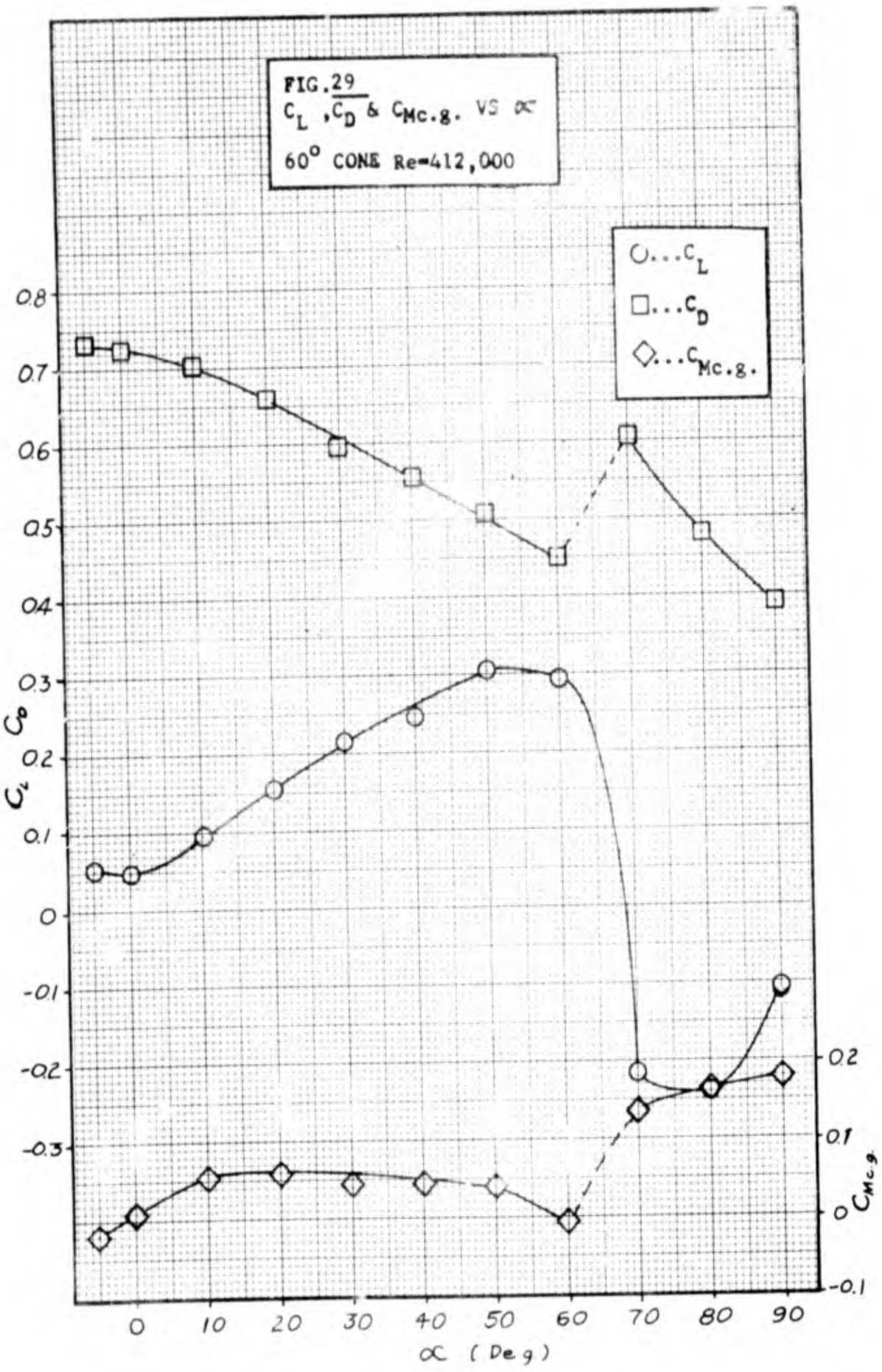
FIG.29
C_L , C_D & $C_{Mc.g.}$ VS α
60° CONE Re=412,000
○...C_L
□...C_D
◇...$C_{Mc.g.}$
0.8
0.7
0.6
0.5
0.4
0.3
0.2
0.1
0
-0.1
-0.2
-0.3
C_D C_L
0.2
0.1
0
-0.1
$C_{Mc.g.}$
0
10
20
30
40
50
60
70
80
90
α (Deg)

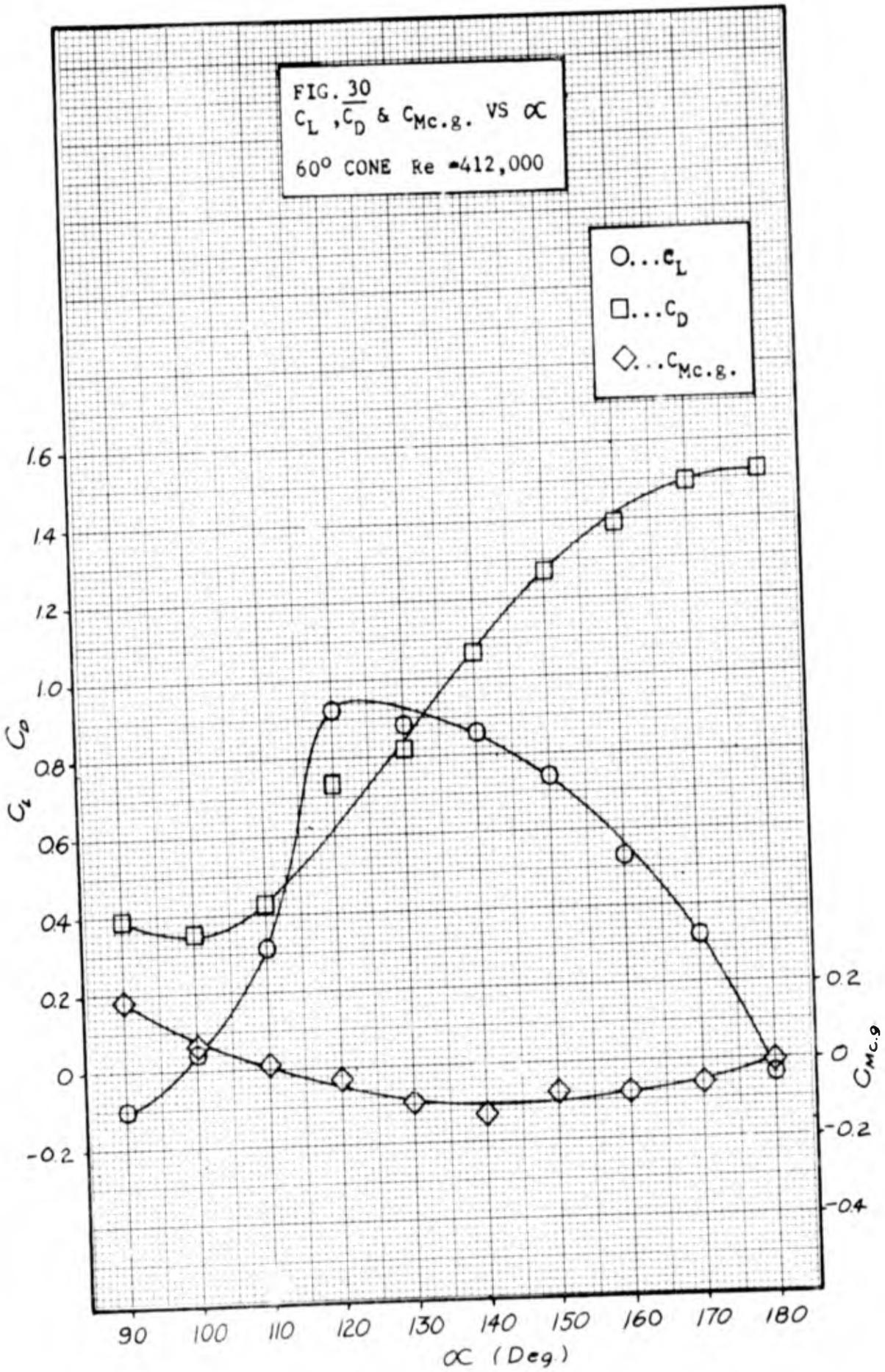
FIG. 30
C_L , C_D & $C_{Mc.g.}$ VS α
60° CONE Re =412,000
O...C_L
□...C_D
◇...$C_{Mc.g.}$
1.6
1.4
1.2
1.0
0.8
0.6
0.4
0.2
0
-0.2
C_L C_D
0.2
0
-0.2
-0.4
$C_{Mc.g}$
90
100
110
120
130
140
150
160
170
180
α (Deg)

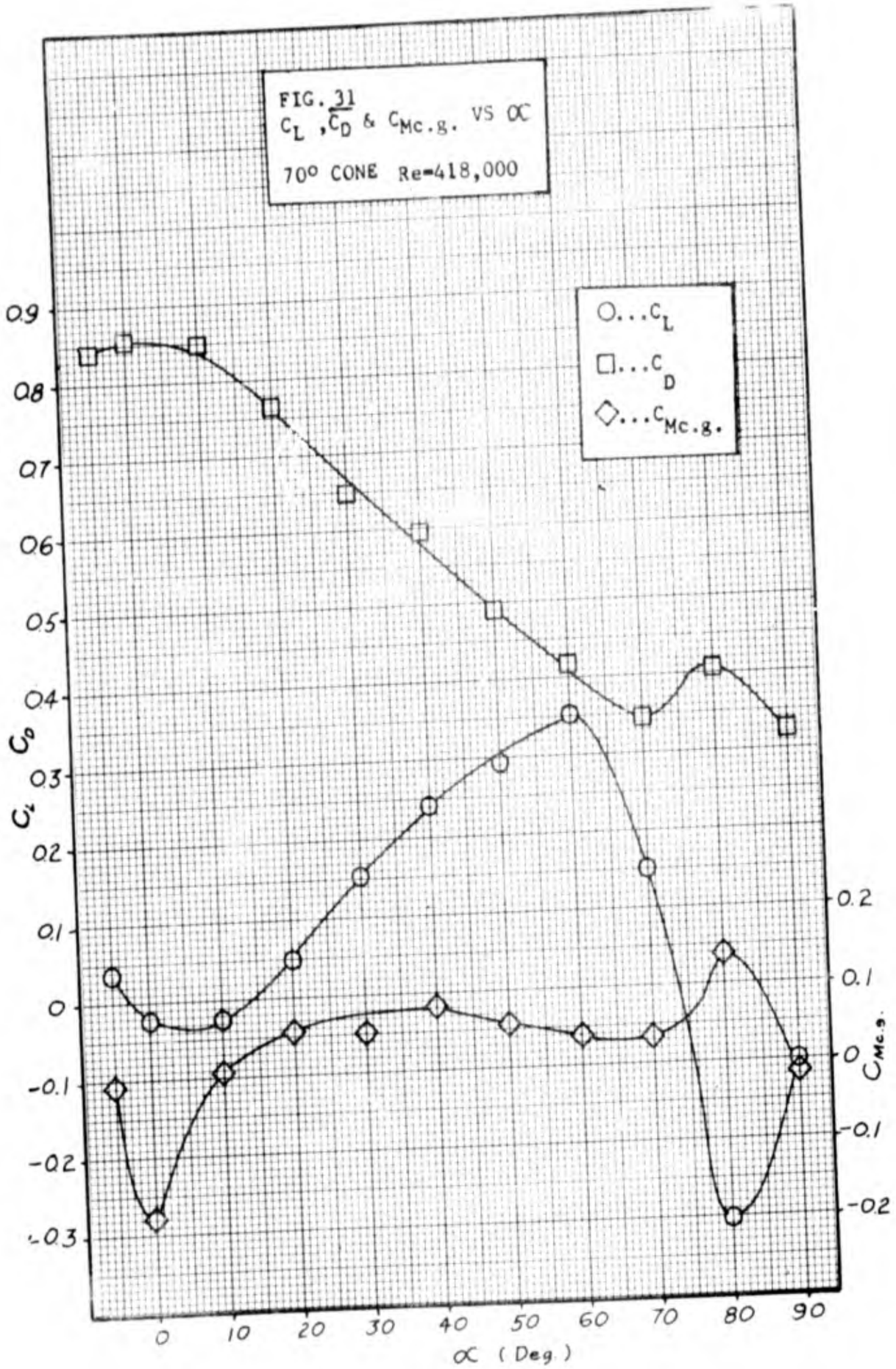
FIG. 31
C_L , C_D & $C_{Mc.g.}$ VS ∝
70° CONE Re=418,000
O...C_L
□...C_D
◇...$C_{Mc.g.}$
0.9
0.8
0.7
0.6
0.5
0.4
0.3
0.2
0.1
0
-0.1
-0.2
-0.3
C_D
C_L
0.2
0.1
0
-0.1
-0.2
$C_{Mc.g.}$
0
10
20
30
40
50
60
70
80
90
∝ (Deg)

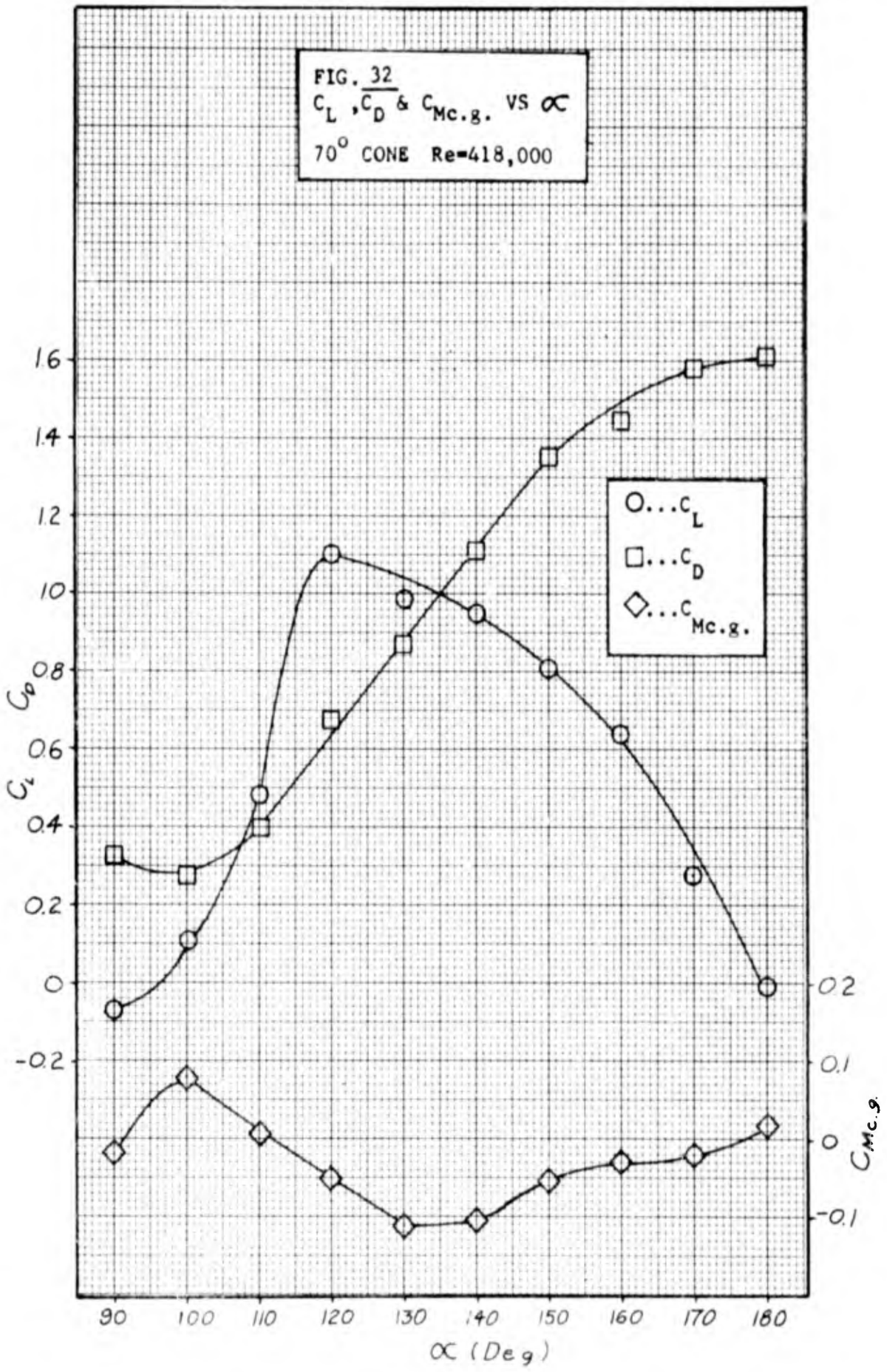
FIG. 32
C_L, C_D & $C_{Mc.g.}$ VS α
70° CONE Re=418,000
O...C_L
□...C_D
◇...$C_{Mc.g.}$
1.6
1.4
1.2
1.0
0.8
0.6
0.4
0.2
0
-0.2
C_L, C_D
0.2
0.1
0
-0.1
$C_{Mc.g.}$
90
100
110
120
130
140
150
160
170
180
α (Deg)

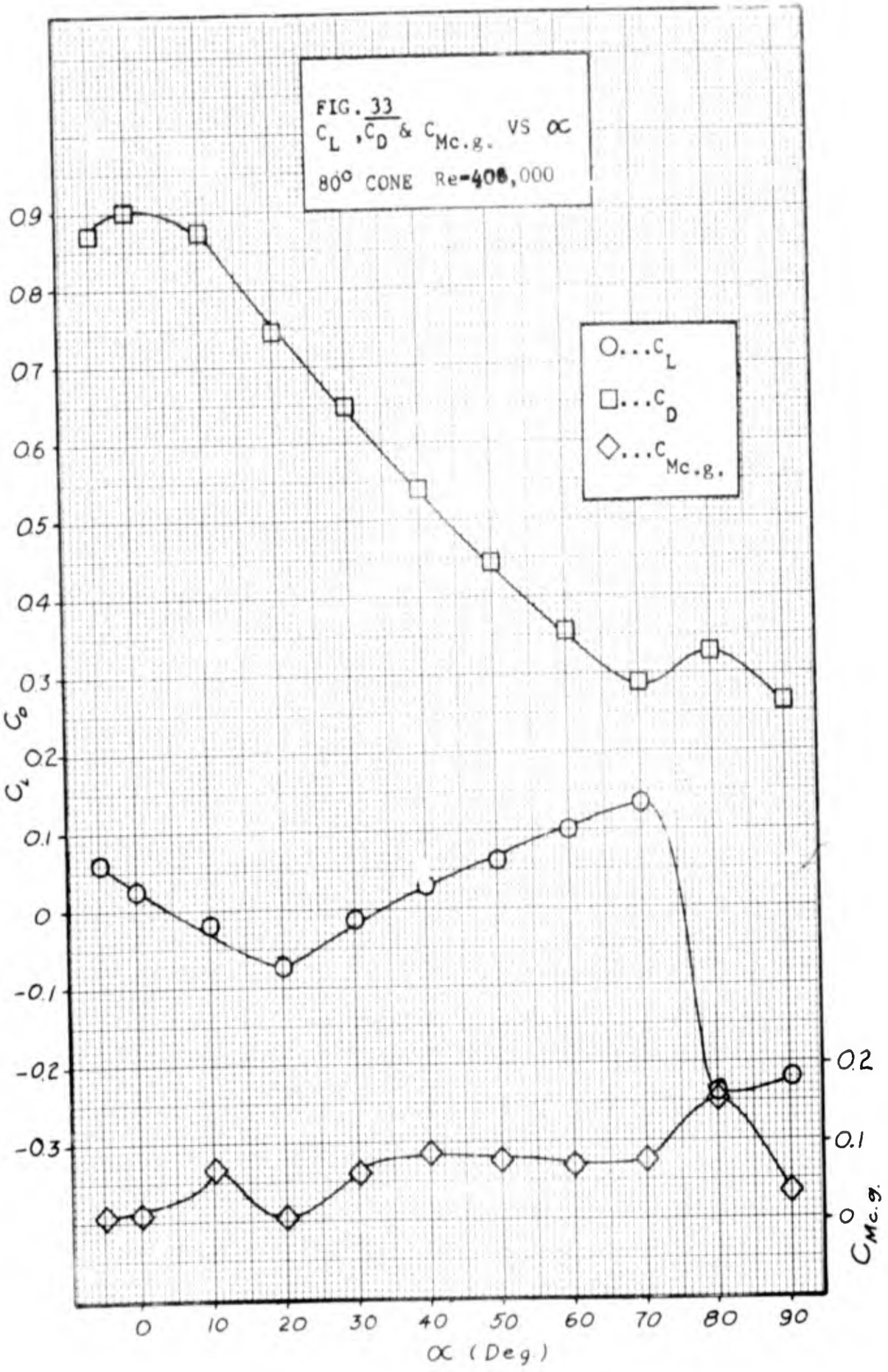
FIG. 33
C_L, C_D & $C_{Mc.g.}$ VS α
80° CONE Re-408,000
O...C_L
□...C_D
◇...$C_{Mc.g.}$
0.9
0.8
0.7
0.6
0.5
0.4
0.3
0.2
0.1
0
-0.1
-0.2
-0.3
C_D, C_L
0.2
0.1
0
$C_{Mc.g.}$
0
10
20
30
40
50
60
70
80
90
α (Deg.)

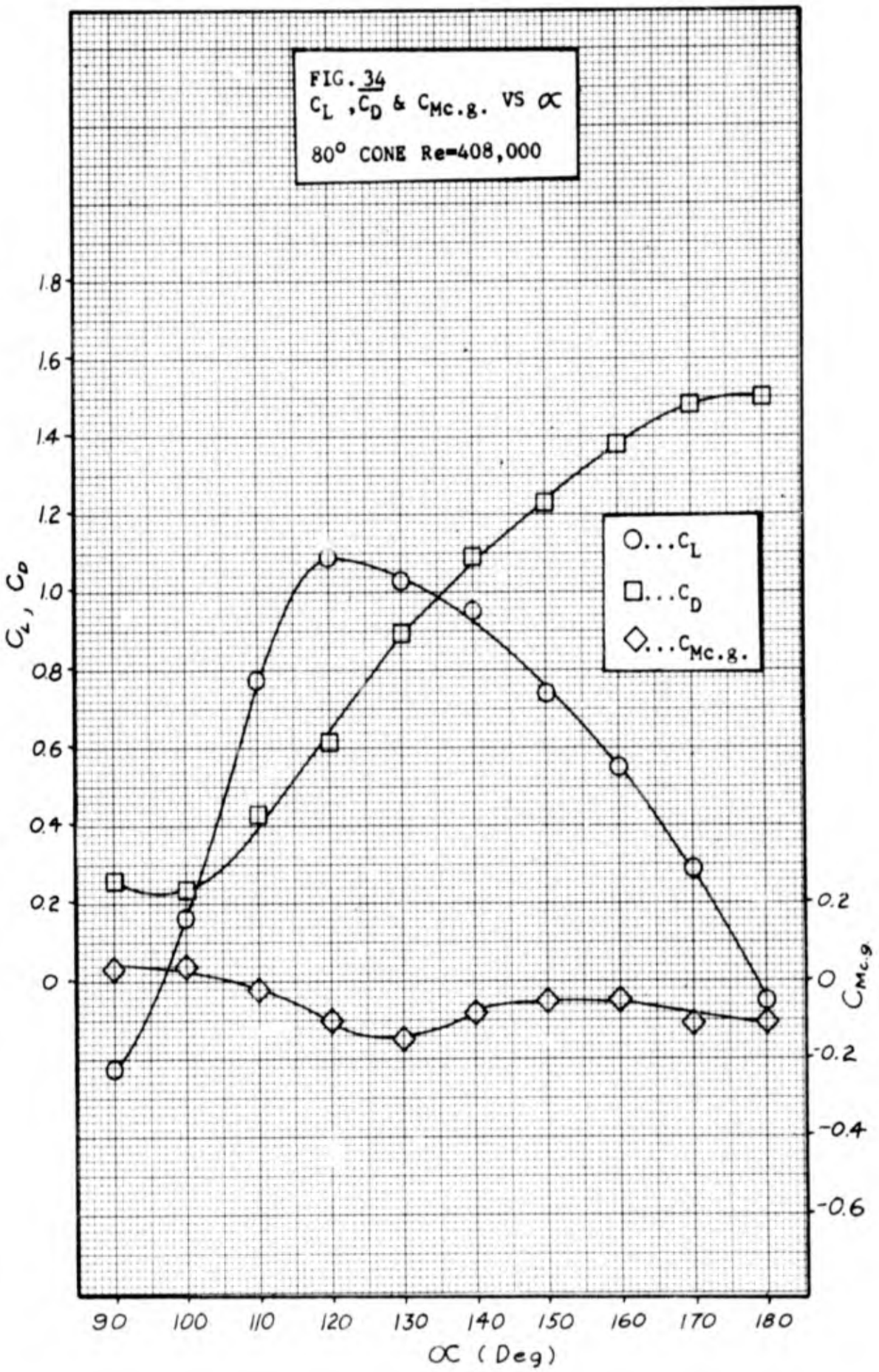
FIG. 34
C_L , C_D & $C_{Mc.g.}$ VS α
80° CONE Re=408,000
O...C_L
□...C_D
◇...$C_{Mc.g.}$
C_L, C_D
$C_{Mc.g}$
α (Deg)
1.8
1.6
1.4
1.2
1.0
0.8
0.6
0.4
0.2
0
-0.2
-0.4
-0.6
90
100
110
120
130
140
150
160
170
180

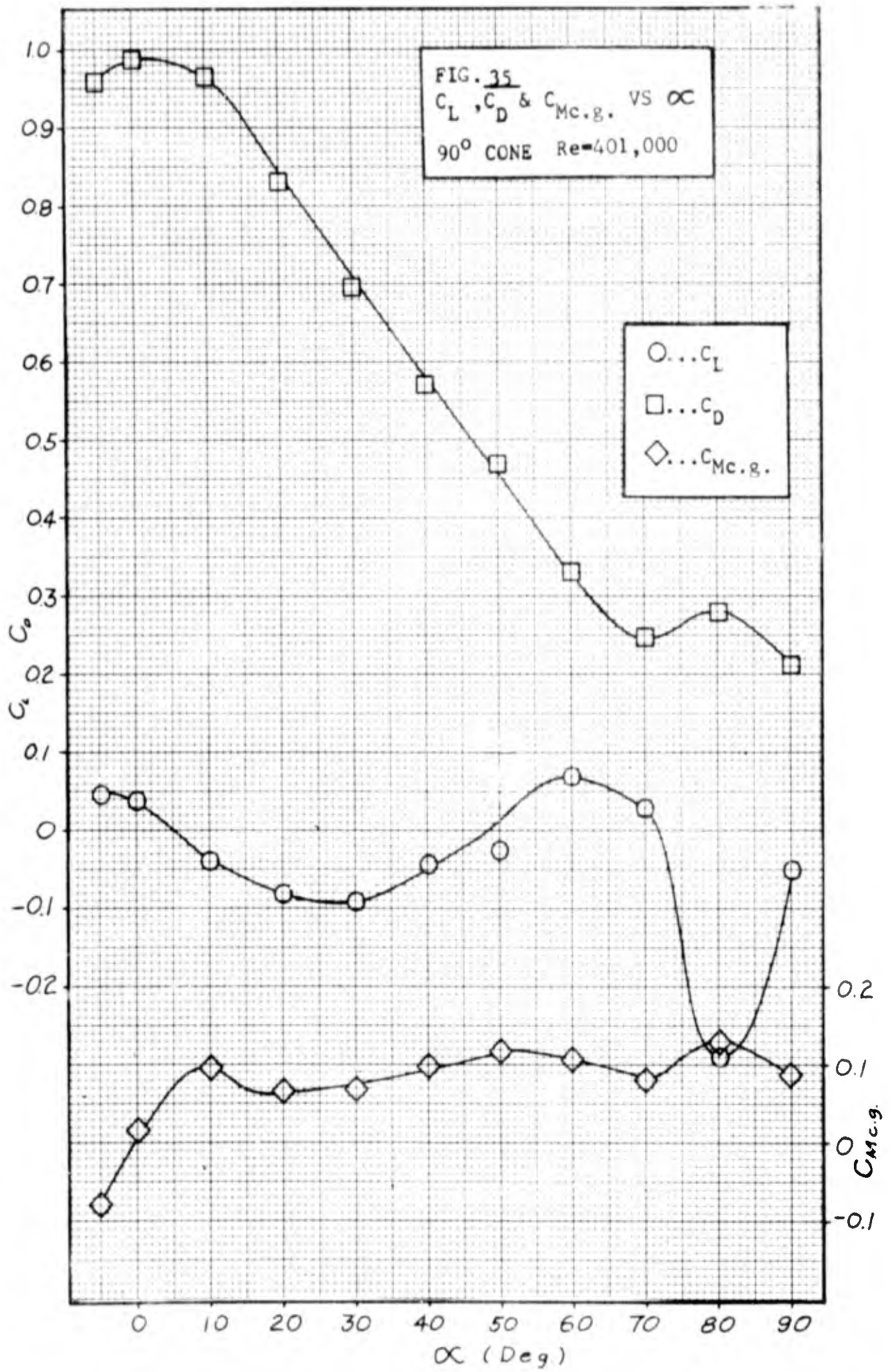
FIG. 35
C_L, C_D & $C_{Mc.g.}$ VS α
90° CONE Re=401,000
O...C_L
□...C_D
◇...$C_{Mc.g.}$
1.0
0.9
0.8
0.7
0.6
0.5
0.4
0.3
0.2
0.1
0
-0.1
-0.2
C_L, C_D
0.2
0.1
0
-0.1
$C_{Mc.g.}$
0
10
20
30
40
50
60
70
80
90
α (Deg)

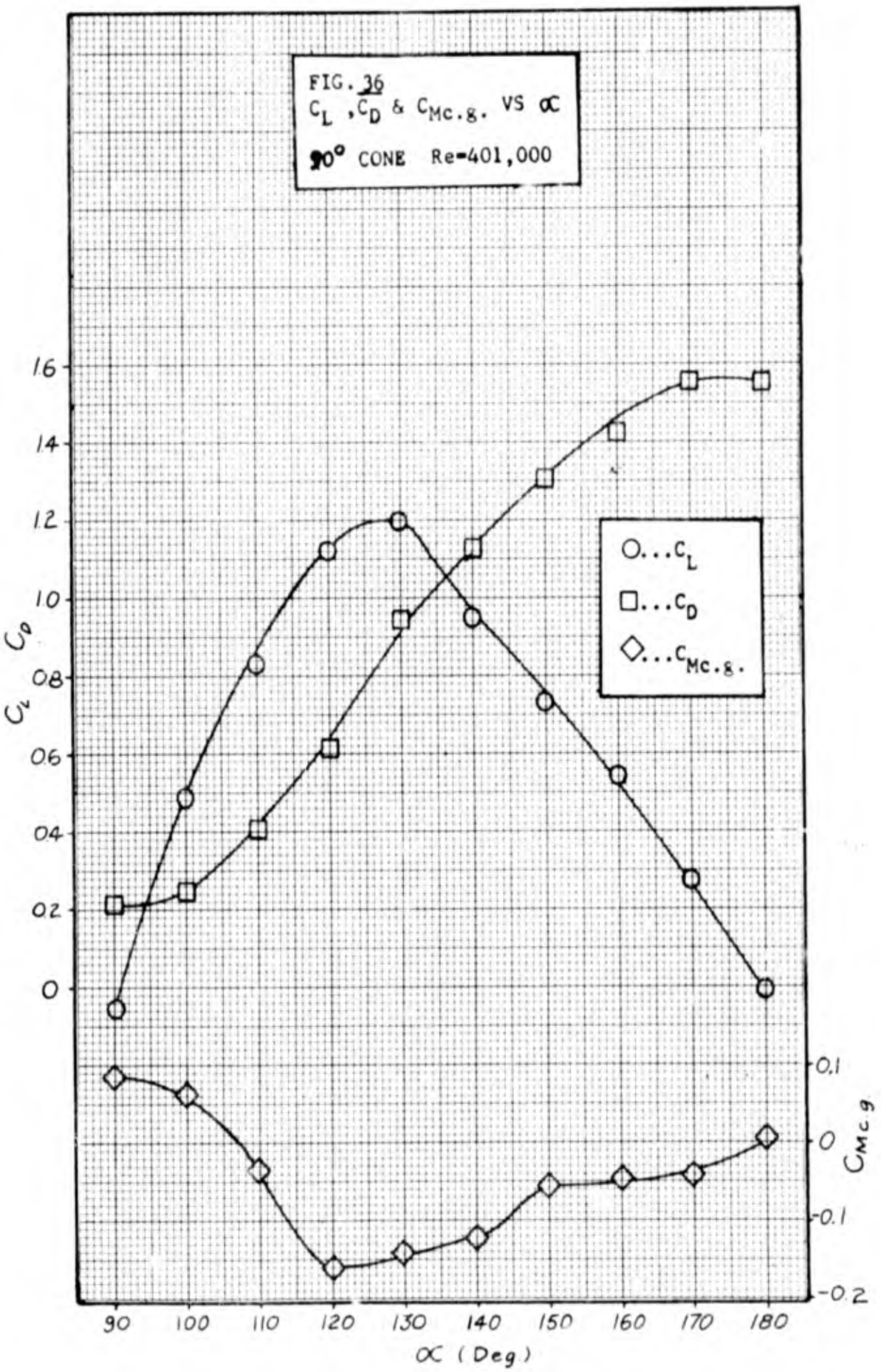
FIG. 36
C_L , C_D & $C_{Mc.g.}$ VS α
90° CONE Re=401,000
O...C_L
□...C_D
◇...$C_{Mc.g.}$
C_L C_D
16
14
12
10
08
06
04
02
0
0.1
0
-0.1
-0.2
$C_{Mc.g}$
90
100
110
120
130
140
150
160
170
180
α (Deg)

Appendix B

Sample Calculations

The following equations were obtained almost entirely from Wind Tunnel Testing by A. Pope (Ref 4:337). Exceptions are the calibration corrections for the tunnel balance and the moment coefficient about the center of gravity of the cone. The numbers used in the sample calculations were those of the 60^{o} cone set at zero angle of attack. Also, the wake blocking was assumed to be constant.

Tunnel Blockage Factor

$$e = (MFA + SFA)/4C$$

$$e = (9.42 + 5.1)/4(150)$$

$$e = 0.0242$$

Corrected Dynamic Pressure

$$q = q_u\ (1 + 2e)$$

$$q = 75(1 + 0.0484)$$

$$q = 78.63\ lb/ft^2$$

Corrected Lift Coefficient

$$C_L = C_L'(1 - \tau_2 \delta(S/C)(57.3) \cdot a)$$

$$C_L' = L/qS$$

where $L = (L_s + I_m + L_m) - (L_s + I_m)$

$$L = (0.71) - (0.46)$$

$$L = 0.25\ lb.$$

$$C_L' = 0.25/(78.63)(9.42/144)$$

$$C_L' = 0.049$$

$\tau_2 = 0.1$ (Ref 4:318)

$\delta = 0.125$ (Ref 4:297)

$C_L = 0.049\left(1 - (0.1)(0.125)(0.0628)(57.3)(0.297)\right)$

$C_L = 0.049\ (0.9866)$

$C_L = 0.052$

Corrected Angle of Attack

$\alpha = \alpha_u + (i + \tau_2)\,\delta\,(S/C)\,C_L'\,(57.3)$

$\alpha = 0 + (1 + 0.1)(0.125)(0.0628)(0.049)(57.3)$

$\alpha = 0.02^\circ$

Angle of attack could only be set to within $\pm 0.1^\circ$ and therefore, this correction was neglected.

Corrected Drag Coefficient

$C_D = (D - \Delta D_B)/(q)\,S + \delta\,(S/C)\,C_L^2$

where $D = 1.01\left((D_s + I_m + D_m) - (D_s + I_m)\right) + D_b$

$D_b = -\,dp/dx(V)$

$dp/dx = -0.3(lb/ft^2)/ft$ (Ref 2: 27)

$V = (9.4/1728)ft^3$

$D_b = -(-0.3)(9.4/1728)$

$D_b = 0.0016$ lb

This was less than the accuracy of the scale and was neglected.

$D = 1.01\left((4.13) - (0.43)\right)$

$D = 3.74$ lb

$\Delta D_B = D\left((K_3\tau_1 V)/\ C^{3/2}\right)$

$K_3 = 1.38$ (Ref 4:289)

$\tau_1 = 0.795$ (Ref 4:289)

$$\Delta D_B = 3.74\left((1.38)(0.75)(9.4)/\ 1835\right)$$

$$\Delta D_B = 0.03\ \text{lb}$$

$$C_D = (3.74 - 0.03)/\ 78.63(9.42/\ 144) + 0.125(0.0628)(0.048)^2$$

$$C_D = 0.722 + 0.0000181^*$$

$$C_D = 0.722$$

* This term was neglected

Corrected Pitching Moment Coefficient

Pitching Moment Coefficient About the Trunion

$$C_{M_{tr}} = M_{tr}/\ qSd - 0.25\tau_2\,\delta\,(S/C)(57.3)\cdot\, aC_L'$$

$$C_{M_{tr}} = (o.51)/(78.63)(9.42/\ 144)(3.46) - (0.25)(0.1)(0.125)(0.0628)$$
$$\times(57.3)(0.297)(0.049)$$

$$C_{M_{tr}} = 0.029 - 0.00017^*$$

$$C_{M_{tr}} = 0.029$$

* This term was neglected

Pitching Moment Coefficient About the Center of Gravity of the Cone Straight Sting

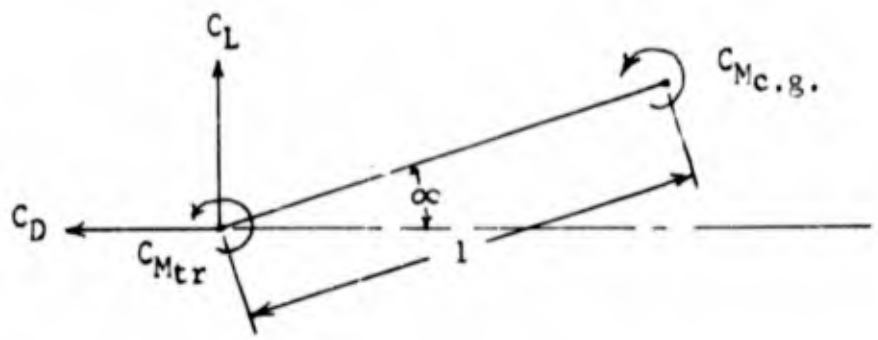

$$C_{M_{c.g.}} = 1/d\ (C_L \cos\alpha + C_D \sin\alpha) - C_{M_{tr}}$$

$$C_{M_{c.g.}} = (3/\ 3.46)\left[(0.048)(1) + (0.722)(0)\right] - C_{M_{tr}}$$

$$C_{M_{c.g.}} = 0.042 - 0.019$$

$$C_{M_{c.g.}} = 0.013$$

Bent Sting

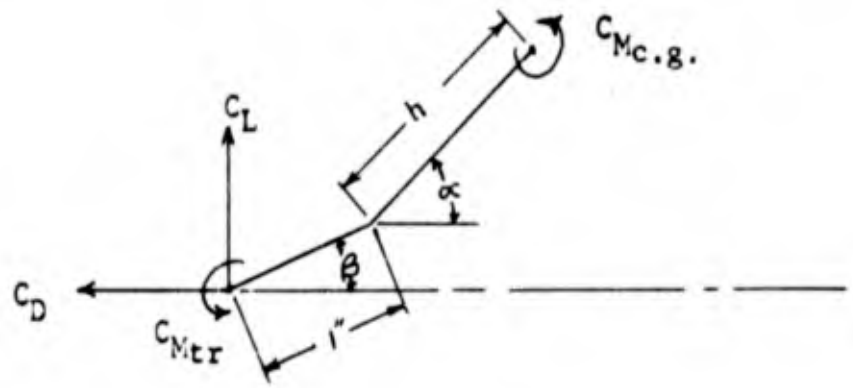

$$C_{M_{c.g.}} = (C_L/\ d)(\cos\beta + h\cos\alpha) + (C_D/\ d)(\sin\beta + h\sin\alpha) - C_{M_{tr}}$$

Calculation of Reynolds Number

$$R_e = (2q)^{\frac{1}{2}}\ (d)/\mu$$

where for an average tunnel temperature of 100° F. and a tunnel pressure of 29.4 in. Hg.

$$\mu = 0.397 \times 10^{-6}\ \text{lb-sec/ft}^2 \qquad \text{(Ref 5 :8)}$$

$$\rho = 0.00214\ \text{lb-sec}^2/\text{ft}^4$$

$$R_e = \left[(2)(78.63)(0.00214)\right]^{\frac{1}{2}}\ (3.46)/\ 0.397 \times 10^{-6}$$

$$R_e = 412{,}000$$

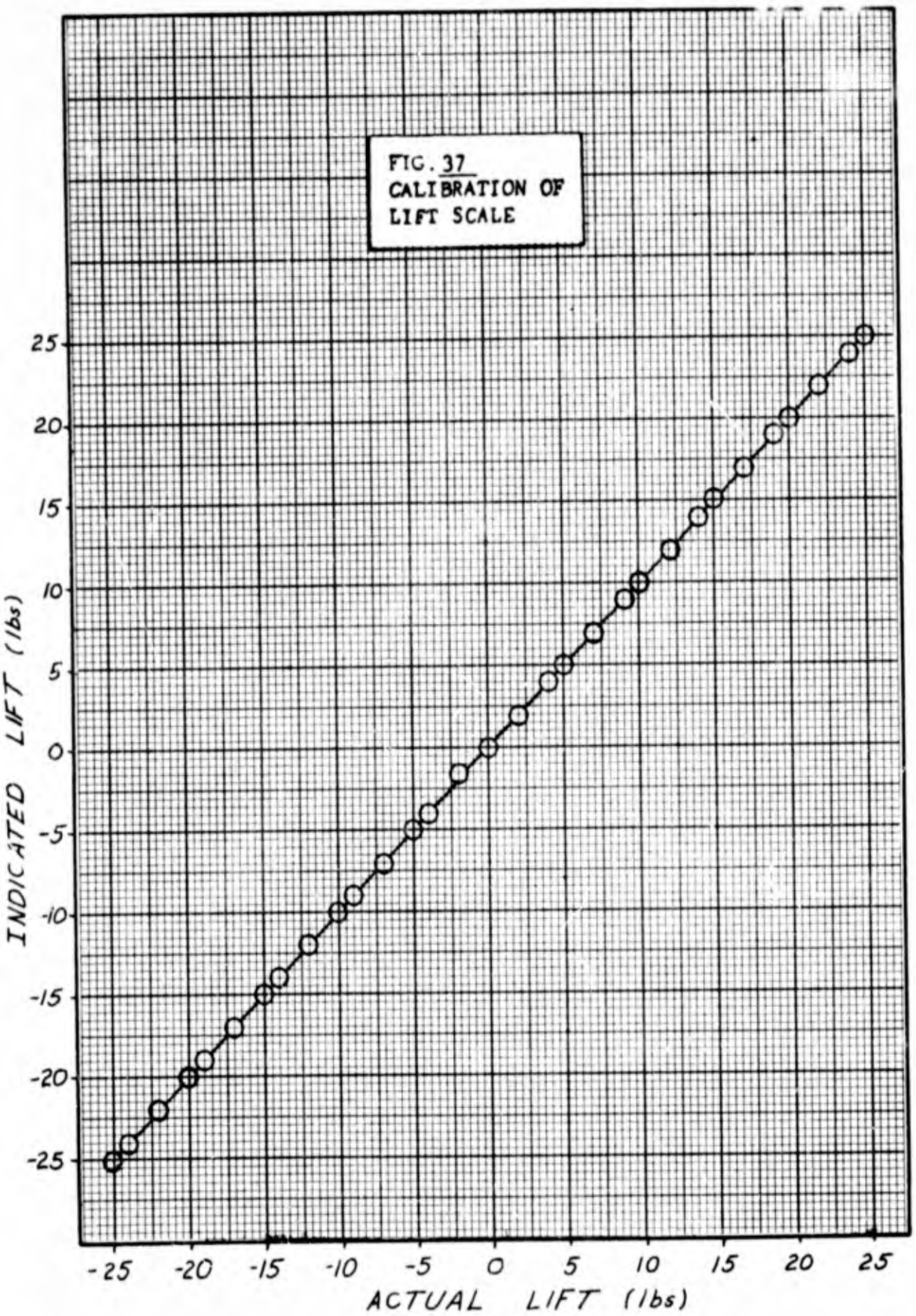
FIG. 37
CALIBRATION OF
LIFT SCALE
INDICATED LIFT (lbs)
25
20
15
10
5
0
-5
-10
-15
-20
-25
-25 -20 -15 -10 -5 0 5 10 15 20 25
ACTUAL LIFT (lbs)

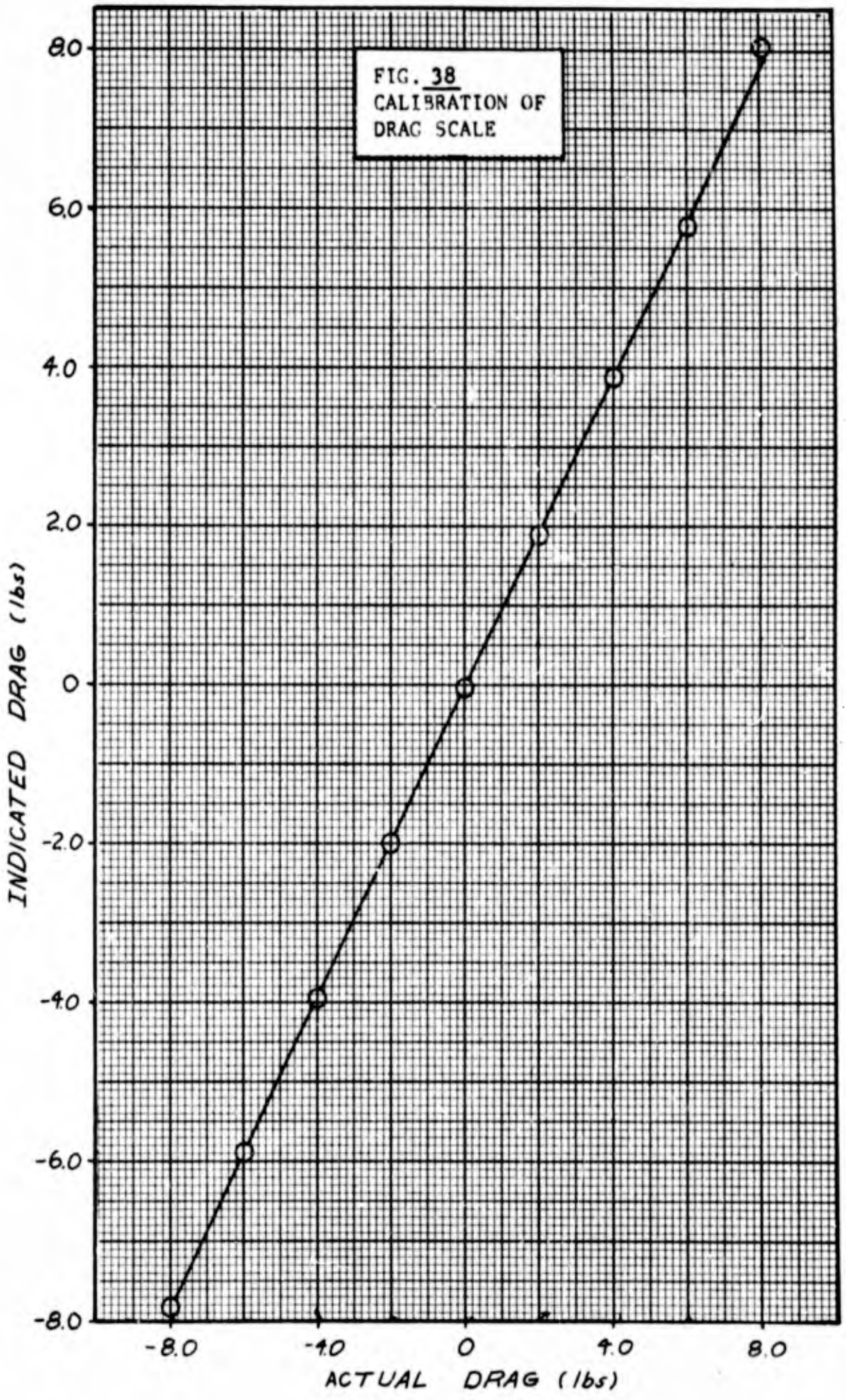

FIG. 38
CALIBRATION OF
DRAG SCALE

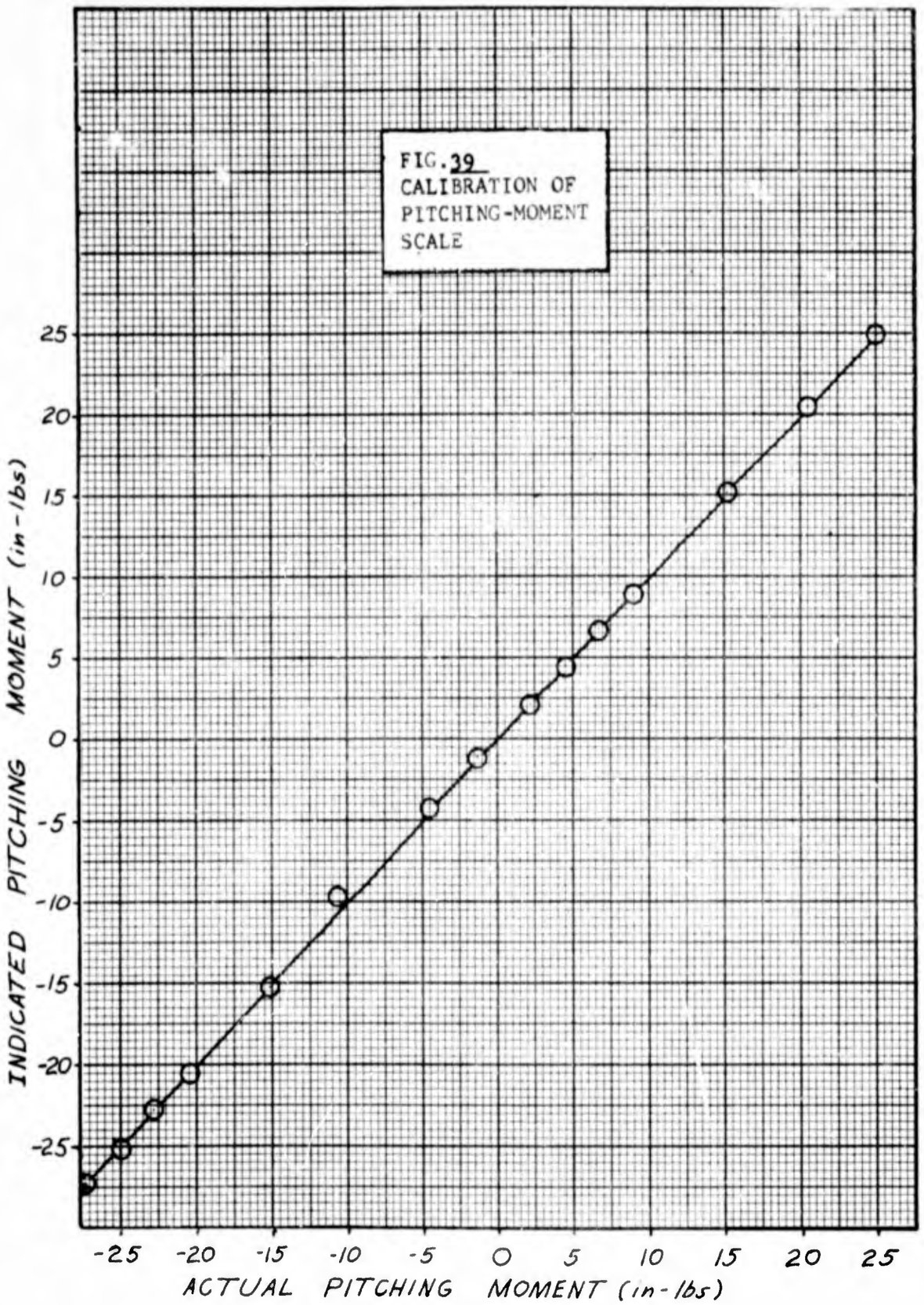
FIG. 39
CALIBRATION OF
PITCHING-MOMENT
SCALE
INDICATED PITCHING MOMENT (in-lbs)
25
20
15
10
5
0
-5
-10
-15
-20
-25
-25 -20 -15 -10 -5 0 5 10 15 20 25
ACTUAL PITCHING MOMENT (in-lbs)

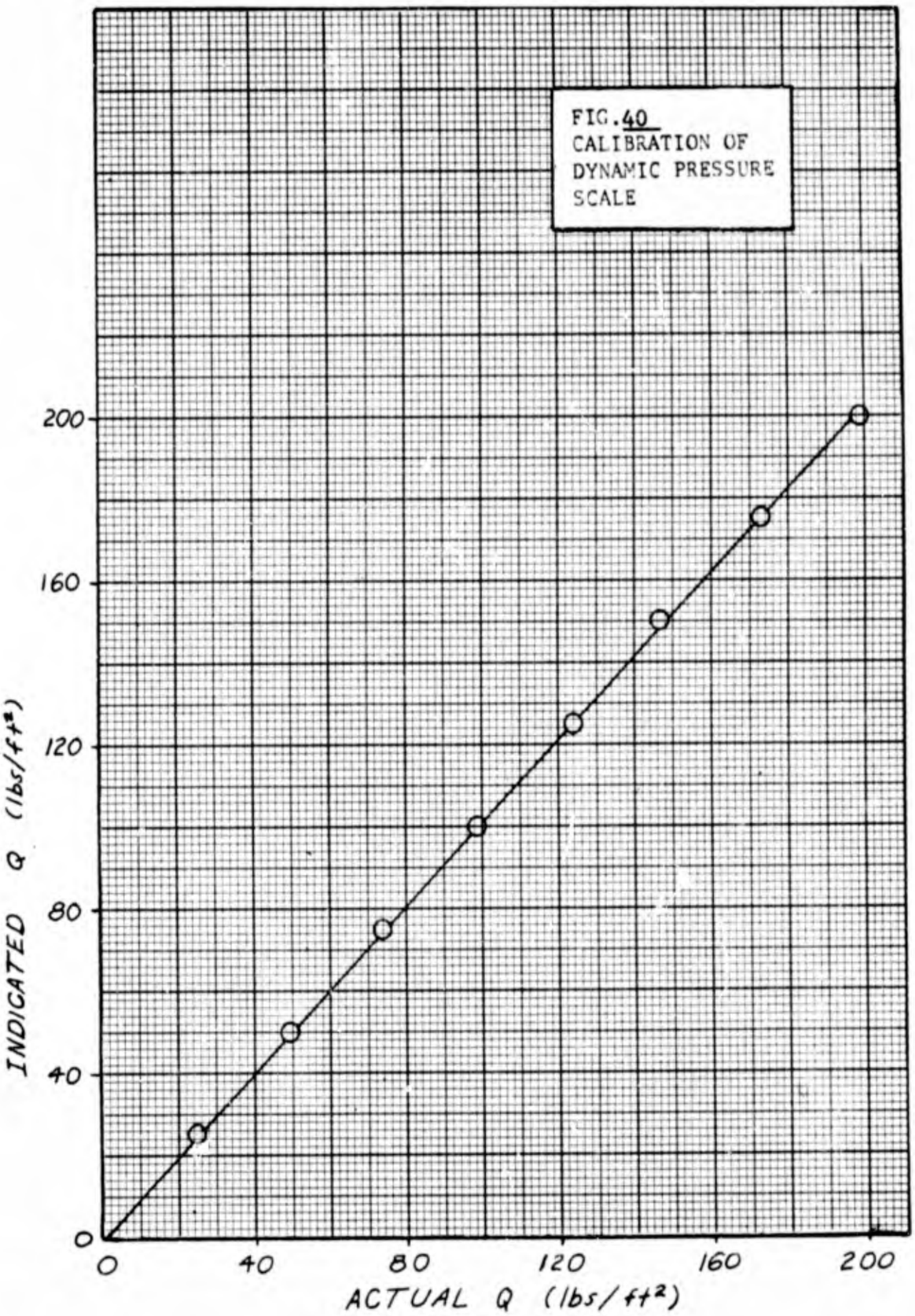
FIG. 40
CALIBRATION OF
DYNAMIC PRESSURE
SCALE
INDICATED Q (lbs/ft²)
ACTUAL Q (lbs/ft²)
0
40
80
120
160
200

Appendix C

Table III. Specifications of Cones

Cone Apex Angle (deg.)	Length (in.)	Diameter (in.)	Base Area ($in.^2$)	Volume ($in.^3$)
10	4	0.70	0.34	0.51
20	4	1.40	1.54	2.05
30	4	2.14	3.60	4.79
40	4	2.90	6.62	8.80
50	4	3.70	10.75	14.33
60	3	3.46	9.42	9.40
70	3	4.20	13.87	13.85
80	2	3.36	8.87	5.91
90	2	4.00	12.58	8.38

Vita

Captain David Litwack was born on [redacted]. He completed secondary schooling in 1950 and graduated in 1955 from New York University with the degree of Bachelor of Aeronautical Engineering and a Reserve Commission in the United States Air Force. He entered active duty in 1956 and after completing pilot training, he accepted a Regular Commission in the United States Air Force. Prior to entering the Air Force Institute of Technology, he served as an all-weather interceptor pilot in the Air Defense Command and the Alaskan Air Command.

Permanent address: [redacted]

This thesis was typed by Mrs. Yvette A. Litwack